Lithos 356–357 (2020) 105302

Contents lists available at ScienceDirect

Lithos

journal homepage: www.elsevier.com/locate/lithos

Silurian anorogenic basic and acidic magmatism in Northwest Turkey: Implications for the opening of the Paleo-Tethys

Gültekin Topuz [a,*], Osman Candan [b], Aral I. Okay [a], Albrecht von Quadt [c], Malik Othman [d], Thomas Zack [e,f], Jiamin Wang [g]

[a] Avrasya Yer Bilimleri Enstitüsü, İstanbul Teknik Üniversitesi, TR34469 Maslak, İstanbul, Turkey
[b] Jeoloji Mühendisliği Bölümü, Dokuz Eylül Üniversitesi, Tınaztepe Yerleşkesi, Buca, İzmir, Turkey
[c] Department of Earth Sciences, Institute of Geochemistry and Petrology, ETH Zurich, Clausiusstrasse 25, CH-8092 Zurich, Switzerland
[d] Faculty of Science, Geology Department, Misurata University, Misurata, Libya
[e] Department of Earth Sciences, University of Gothenburg, Gothenburg, Sweden
[f] Department of Earth Sciences, University of Adelaide, Australia
[g] State Key Laboratory of Lithospheric Evolution, Institute of Geology and Geophysics, Chinese Academy of Sciences, 19 Beitucheng West Road, Chaoyang District, 100029 Beijing, China

ARTICLE INFO

Article history:
Received 7 August 2019
Received in revised form 18 November 2019
Accepted 18 November 2019
Available online 21 November 2019

Keywords:
U—Pb zircon dating
Zircon Hf isotopes
Paleo-Tethys
Silurian magmatism
Armorica
Sakarya Zone
Turkey

ABSTRACT

The Sakarya Zone (northern Turkey) is a Gondwana-derived continental block accreted to northern Laurussia during the Carboniferous, and is regarded as the eastward extension of Armorica. Timing of its detachment from the northern margin of Gondwana, thus opening of the Paleo-Tethys, is poorly known. Here, we report on metagranite and amphibolite with Silurian igneous crystallization ages from the Early Carboniferous high-temperature/middle to low-pressure amphibolite-facies metamorphic rocks of the Sarıcakaya Massif within the Sakarya Zone (NW Turkey). The metagranite-amphibolite complex is exposed mainly along the southern margin of the Sarıcakaya Massif over an area of ca. 12 km by 1.5 km. The metagranite contains preserved domains of porphyric texture, indicative of derivation from a former granite porphyry. The amphibolite is devoid of any relict igneous texture. Both the metagranite and amphibolite are crosscut by late up to 50 cm thick felsic veins. Uranium-Pb dating on igneous zircons from both metagranite and amphibolite yielded Silurian ages of ca. 419 ± 6 to 434 ± 7 Ma (2σ), and on those from a felsic vein an age of 319 ± 5 Ma (2σ) (Late Carboniferous). Geochemically, amphibolite displays anorogenic transitional tholeiitic to alkaline signatures. Initial εHf values of the igneous zircons from both metagranite and amphibolite show a large variation with medial values of -16 to -9 and $+3$ to $+6$, respectively. Thus, the protoliths of amphibolite were derived from melts of depleted mantle, and those of the metagranite, on the other hand, from melts of reworked crustal material. We suggest that the Silurian anorogenic magmatism is related to a rifting event at the northern margin of Gondwana leading to the detachment of the Sakarya Zone and hence placing an age on the initial opening of the Paleo-Tethys. This interpretation is based on (i) the presence of Late Silurian to Devonian deep-sea sedimentary blocks in the Paleo-Tethyan accretionary complexes, and (ii) the resemblance of the U—Pb age spectra of detrital zircons in the metaclastic sequence of the Sarıcakaya Massif to those of Cambro-Ordovician sandstones in Jordan (Gondwana), and (iii) the local occurrence of anorogenic A-type granites of Late Ordovician-Silurian age in the Anatolide-Tauride Block, a continental block which rifted from Gondwana during the Early Triassic. Wholly anorogenic nature of the Late Ordovician to Silurian igneous rocks in the Sarıcakaya Massif and reported in literature does not support the opening of the Paleo-Tethys as back-arc ocean, as suggested in most paleogeographic reconstructions.

1. Introduction

The Variscan orogeny is considered to have formed by (i) the accretion of Gondwana-derived terrane Armorica to Laurussia during the Early Carboniferous, and (ii) by subsequent continental collision of Gondwana with the amalgamated Eurasia (Fig. 1) (e.g. Franke, 2000; Kroner and Romer, 2013; Matte, 2001; Nance and Linnemann, 2008; Stampfli and Borel, 2002; von Raumer and Stampfli, 2008;

* Corresponding author.
E-mail addresses: topuzg@itu.edu.tr (G. Topuz), osman.candan@deu.edu.tr (O. Candan), okay@itu.edu.tr (A.I. Okay), albrecht.vonquadt@erdw.ethz.ch (A. von Quadt), m.othman@sci.misuratau.edu.ly (M. Othman), thomas.zack@gu.se (T. Zack), wangjiamin@mail.iggcas.ac.cn (J. Wang).

https://doi.org/10.1016/j.lithos.2019.105302

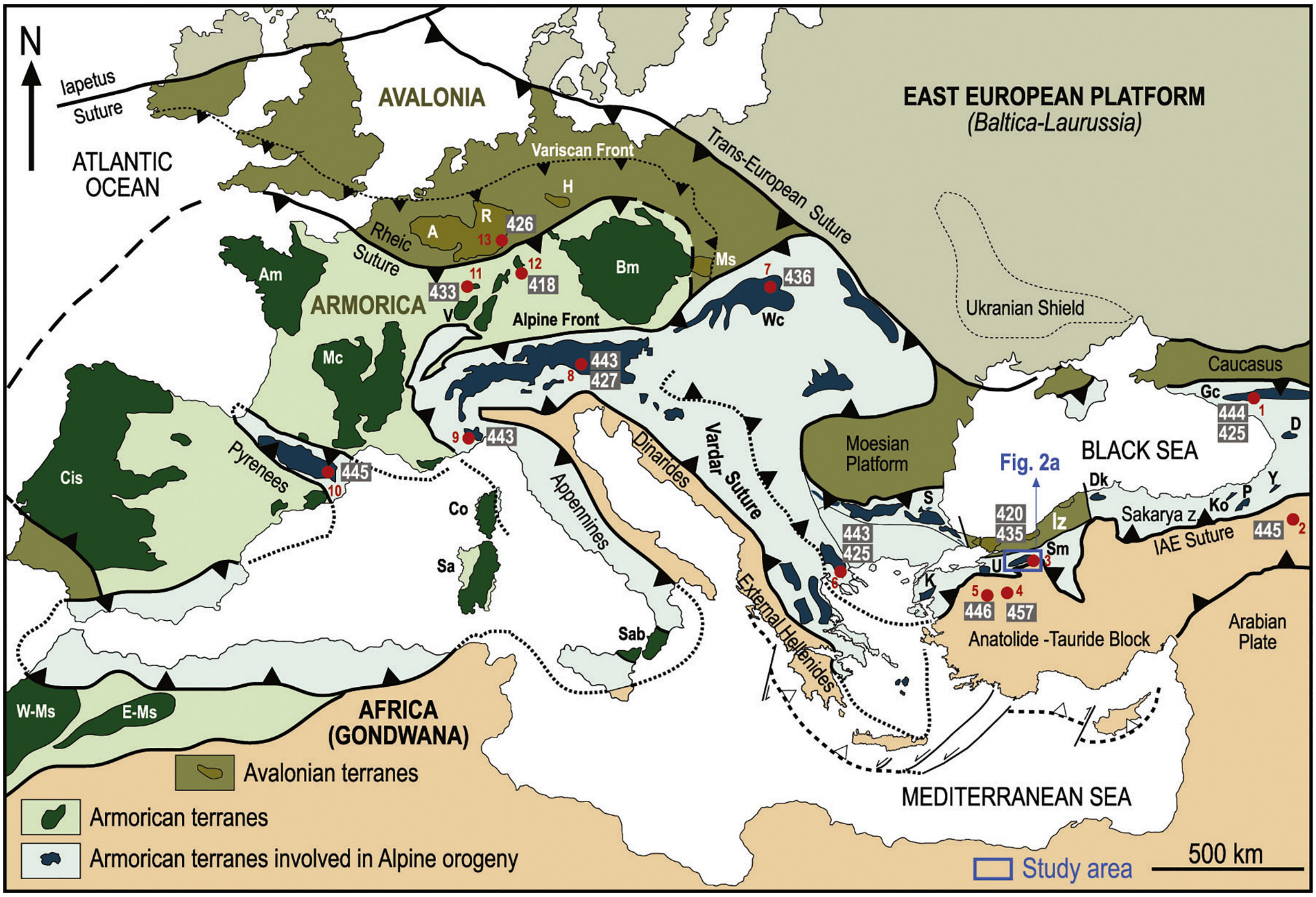

Fig. 1. Simplified tectonic map of the Europe and neighboring areas, showing main Phanerozoic sutures (modified after Neubauer, 2002; Okay et al., 2008a; von Raumer et al., 2013; Schmid et al., 2019). Triangle on the sutures indicate subduction polarity. Red dots stand for the localities of Silurian magmatism. A: Ardennes; Am: Armorica; Bm: Bohemian Massif; Cis: Central Iberian; Co: Corsica; D: Dzirula; Dk: Devrekani; Gc: Greater Caucasus; H: Harz; Iz: Istanbul zone; K: Kazdağ; Ko: Kurtoğlu; Mc: Massive Central; Ms.: Moravia-Silesia; W-Ms: Western Meseta; *E*-Ms: Eastern Meseta; P: Pulur; R: Rhenisch massif; S: Strandja; Sab: Sicilian-Apulian basements; Sa: Sardinia; Sm: Sarıcakaya Massif; U: Uludağ; V: Vosges; Wc: Western Carpathians; Y: Yusufeli. Radiometric ages are taken from [1]Somin (2011), [2]Topuz et al., 2017, [3]this study, [4]Okay et al. (2008a), [5]Özbey et al. (2013), [6]Himmerkus et al. (2009) and Antić et al. (2016), [7]Putiš et al. (2009), [8]Cliff (1980), [9]Rubatto et al. (2001), [10]Casas et al. (2010), [11]Reischmann and Anthes (1996), [12]Dombrowski et al. (1995), and [13]Sommermann et al. (1994).

von Raumer et al., 2013; Winchester and the PACE TMR Network Team, 2002). This continental collision between the Gondwana and Laurussia in North America and Europe resulted in the formation of Pangea during early Permian, and a westerly narrowing oceanic embayment, commonly known as Paleo-Tethys. This broad scheme is complicated (i) by the operation of several large-scale strike faults which led to substantial displacement of magmatic arcs, and (ii) by the fact that parts of the Variscan belt in Europe were later rifted, leading to the opening of several Neo-Tethyan oceanic basins that were closed during the course of the Alpine orogeny (e.g. Schmid et al., 2019).

The geology of Turkey is mainly shaped during the Alpine orogeny. It is made up of several Gondwana-derived continental blocks which were detached from Gondwana, and accreted to Laurussia at different times, followed by the final collision with Gondwana during the Tertiary (Fig. 1) (Okay et al., 2008a, 2008b; Okay and Nikishin, 2015; Okay and Topuz, 2017; Şengör and Yılmaz, 1981). Following the formation of Pangea, the northern continental blocks, the Istanbul and Sakarya zones, were already part of Laurussia, while the Anatolide-Tauride block was located to the south of the Paleo-Tethyan oceanic domain, thus part of Gondwana. The Istanbul Zone is regarded as eastward elongation of Avalonia. The Sakarya Zone is, on the other hand, thought as the eastward elongation of Armorica (Okay et al., 2008a, 2008b; Okay and Topuz, 2017; Ustaömer et al., 2012a, 2012b; Winchester and the Pace TMR Network Team, 2002). In clear distinction to Central Europe, there was no Gondwana-Laurussia collision in the Eastern Mediterranean region during the Variscan Orogeny. To the south, the Sakarya Zone faced an oceanic domain at least from late Silurian to the end-Mesozoic (e.g. Kozur, 1998; Okay et al., 2011).

In this paper we report on the biotite-metagranite and amphibolite with Silurian igneous crystallization ages from the Early Carboniferous high-T/middle to low-P metamorphic rocks from the Sakarya Zone (Sarıcakaya Massif, NW Turkey) (Fig. 1). The geochemical data conclusively show that the protoliths of the amphibolite were derived from anorogenic alkaline to tholeiitic magmas, and those of the biotite-metagranite from crustal melts. In conjunction with the data from literature, we suggest that the anorogenic basic to acidic magmatism in the Sarıcakaya Massif is related to the rifting event during the Late Ordovician to Silurian, leading to the detachment of the Sakarya Zone from the northern margin of Gondwana, thus to the opening of the Paleo-Tethys.

2. Geological setting

The Sakarya Zone represents a long-lasting active southern continental margin of Laurussia at least from late Paleozoic to end-Mesozoic, related to northward subduction along the Izmir-Ankara-Erzincan suture (Fig. 1; Okay, 2000; Okay et al., 2011; Topuz et al., 2004b, 2013a, 2013b, 2018; Okay and Nikishin, 2015). Closure of the oceanic domain occurred during Paleocene-Early Eocene (e.g., Okay and Şahintürk, 1997; Topuz et al., 2011). Consequently, in the Sakarya Zone accretionary complexes of Permo-Triassic, Jurassic and Cretaceous ages are juxtaposed without any intervening continental fragment. Hence, the Mesozoic Tethys was a continuation of the Paleozoic one (e.g., Okay, 2000; Okay and Nikishin, 2015; Topuz et al., 2013a, 2013b, 2014). Ages of the deep-sea sedimentary blocks in the Paleo-Tethyan accretionary complexes, the Karakaya Complex in the Sakarya Zone and the Karareis Formation in the Karaburun peninsula, date back to Devonian to Late Silurian, respectively (Kozur, 1998; Okay et al., 2011). This line of evidence suggests that the age of the Paleo-Tethyan oceanic domain dates back at least to Devonian to Late Silurian times.

The Sakarya Zone has a pre-Jurassic continental basement, which forms isolated inliers beneath the Lower Jurassic volcanic and clastic rocks (Fig. 2); the basement comprises (i) Early to Middle Devonian granites intruding phyllites of unknown age (Aysal et al., 2012a; Okay et al., 1996; Sunal, 2013), (ii) Early Carboniferous high-T/middle to low-P metamorphic rocks intruded by Early Carboniferous to Triassic gabbroic to granitic rocks (Dokuz, 2011; Karslı et al., 2017; Kaygusuz et al., 2016; Nzegge et al., 2006; Topuz et al., 2004a, 2007, 2010; Topuz and Altherr, 2004; Ustaömer et al., 2012a, 2012b), and (iii) subordinate Upper Carboniferous to Lower Permian sedimentary rocks sitting on Early Carboniferous cordierite-bearing rhyolites and phyllites (Dokuz et al., 2017; Okay and Leven, 1996). So far, direct contacts between these units are not observed. Apart from the local presence of the Devonian granites, the pre-Carboniferous geologic evolution of the Sakarya zone is scarcely known. This is partially due to the facts that (i) the upper part of the Carboniferous crust were largely eroded by Early Jurassic time, and (ii) some Carboniferous basement areas were largely reworked during the Alpine orogeny (e.g. Kazdağ, Uludağ and Devrekani massifs) (e.g. Okay et al., 2008c). The Variscan domains are locally well-preserved in areas such as Sarıcakaya, Pulur, Kurtoğlu, Yusufeli in Turkey and Dzirula in Georgia (Mayringer et al., 2011; Rolland et al., 2011; Somin, 2011; Topuz et al., 2004a, 2007; Topuz and Altherr, 2004; Ustaömer et al., 2012a, 2012b) (Fig. 1). The Carboniferous high-T/middle to low-P metamorphism and associated magmatism in the Sakarya Zone are ascribed to a Carboniferous magmatic arc, developed as a consequence of the closure of the Rheic ocean and the collision of the Sakarya Zone with the southern margin of Laurussia during mid-Carboniferous (Okay and Topuz, 2017; Rolland, 2017). This paper presents geochemical and geochronological data on amphibolites and metagranites from the Sarıcakaya Massif (NW Turkey) to constrain their igneous crystallization ages and the tectonic setting of their formation.

3. The Sarıcakaya Massif

The Sarıcakaya Massif (NW Turkey), part of the pre-Liassic continental basement of the Sakarya Zone, forms an E-W trending belt, ~60 km long and ~8 km across, in NW Turkey, and is made up of Early Carboniferous metamorphic rocks which are intruded by Early to Late Carboniferous intrusive rocks (Fig. 3a, b) (Göncüoğlu et al., 2000; İlbeyli et al., 2015; Uğurcan et al., 2019; Ustaömer et al., 2012b). It is unconformably overlain by Lower Jurassic clastic rocks and Upper Jurassic to Lower Cretaceous platform limestone in the north. To the south, it is thrust over the Permo-Triassic accretionary complex and the Eocene sedimentary and volcanic rocks. The metamorphic rocks are frequently crosscut by quartz diorite, hornblende-biotite granite, and cumulate gabbro-peridotite. Contact metamorphism is only marked around the gabbro-peridotite bodies. U—Pb zircon ages of the granites range from 327 to 308 Ma (e.g. Ustaömer et al., 2012b; own data) (see ages on Fig. 3b). In this study we mapped the central part of the Sarıcakaya Massif, 8 km by 12 km (Fig. 3a, b).

The metamorphic rocks of the Sarıcakaya massif in the studied part include amphibolite-facies metaclastic rocks (ca. 40% of the exposure), metagranite (ca. 25%), amphibolite (ca. 15%), and minor marble (≤1%). These metamorphic rocks are frequently crosscut by up to 10 m thick dikes/sills of leucocratic aplite to pegmatite which include muscovite and locally garnet and tourmaline (ca. 20% of the exposure), and show ductile to brittle deformational features. The metaclastic sequence is represented by quartzofeldspathic schist/gneiss, metapelitic gneiss and metaquarzite. The metapelitic gneisses are characterized by mineral assemblages with garnet, sillimanite, biotite, plagioclase, quartz and K-feldspar, indicative of the upper amphibolite-facies conditions. The biotite-metagranite and amphibolite, on which we focus in this study to place constraints on the pre-Carboniferous igneous evolution of the Sakarya Zone, crop out mainly in the southern part of the area

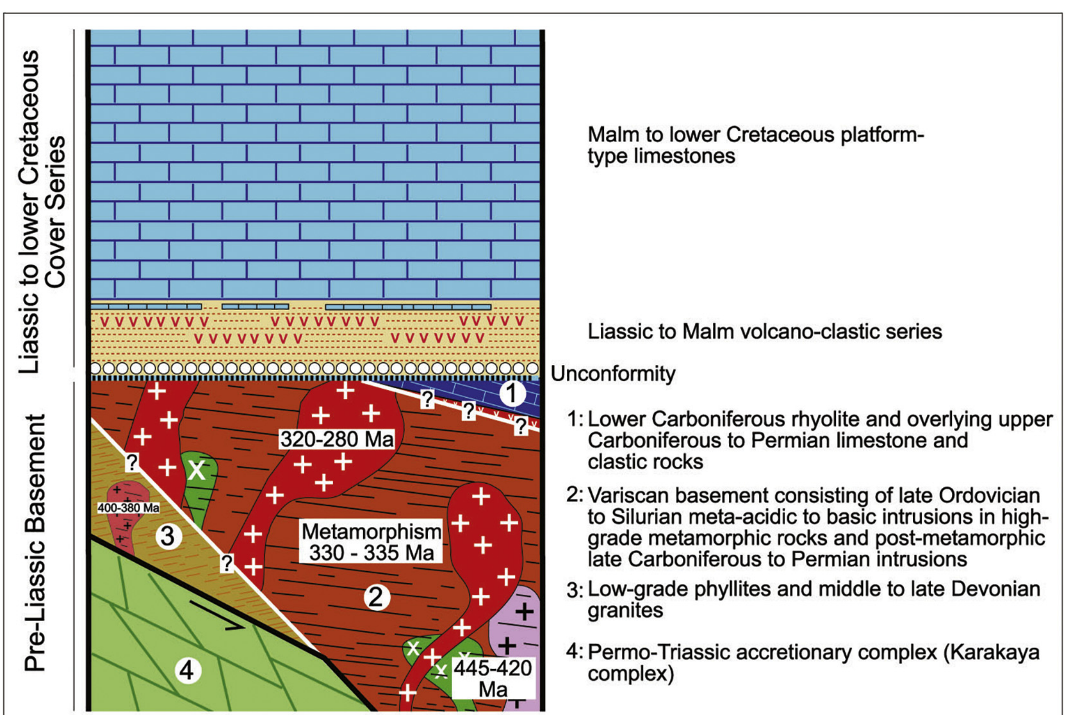

Fig. 2. Columnar section showing the pre-Liassic basement and unconformably overlying Jurassic cover.

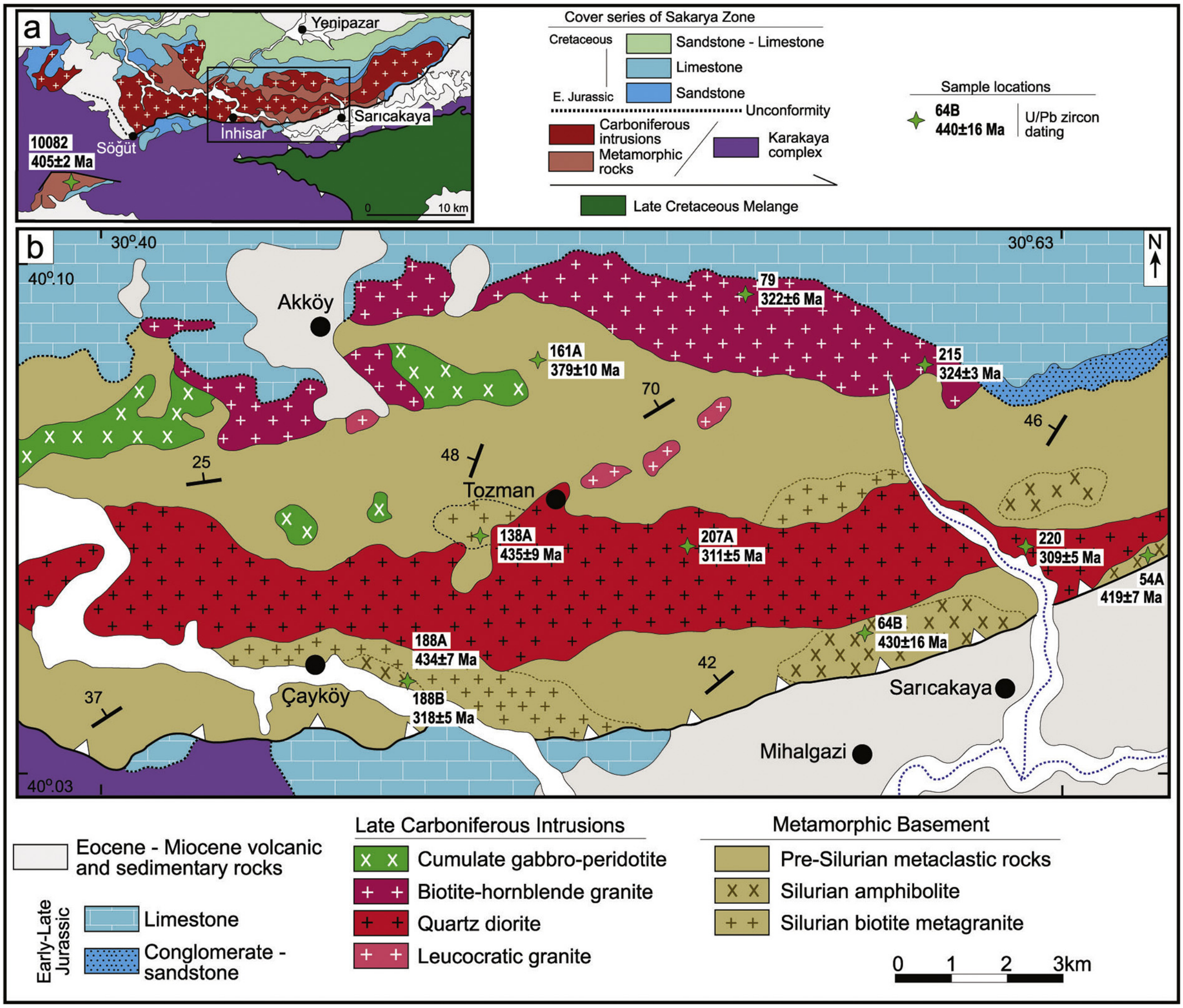

Fig. 3. (a) The geological map of the Sarıcakaya massif and its environs (modified after the geological map of Turkey with the scale of 1/500.000, M.T.A., 2004). (b) Geological map of the middle part of the Sarıcakaya massif (modified after Othman, 2017).

mapped (Fig. 3b). The biotite-metagranite forms the dominant rock type, and occur either over large areas, or as up to 20 m thick premetamorphic intrusive bodies within both amphibolite and metaclastic sequence. Biotite-metagranite displays a well-developed foliation with a blastomylonitic, augen gneissic to ultramylonitic fabric (Fig. 4a–d). In less deformed domains, pre-metamorphic porphyritic texture is still recognizable. As the primary intrusive contact relationship of the biotite-metagranites was largely obscured, biotite-metagranite and quartzo-feldspatic gneiss of the metaclastic sequence are difficult to distinguish in the absence of textural relics, because both are made up of feldspar, quartz and biotite. Hence, the boundaries of the biotite-metagranite are shown in an approximate manner in Fig. 3b. Apart from the main biotite-metagranite, there are additionally two distinct types of metagranitic rocks: two-mica metagranite and hornblende-biotite metatonalite, which are not studied in detail. However, we describe them and provide U—Pb ages of these metaigneous rocks to show that they are not part of the Silurian magmatism. The two-mica metagranite occurs as veins and small stocks up to 20 m in diameter (sample 161A). The hornblende-biotite metatonalite (sample 10082) makes up a substantial portion of another isolated regional metamorphic area around the town of Bozüyük, 15 km to the southwest of the Sarıcakaya Massif, which occupies a comparable structural position as the Sarıcakaya Massif (Fig. 3a).

Amphibolite forms small stocks, ca. 1.5 km long and ca. 0.5 km wide, or up to 50 m thick interlayers/dikes within both biotite-metagranite and metaclastic rocks (Fig. 3b). It is mostly well-foliated, and does not contain any textural relics. Amphibolite locally contains 0.5–50 cm thick foliation-parallel felsic veins, which locally crosscut the foliation (Fig. 4e). In addition, there are diffuse, hornblende-bearing leucosomes within the amphibolite, which are probably related to partial melting of amphibolite (Fig. 4f).

4. Analytical methods

For bulk-rock analyses about 5 kg of amphibolite and biotite-metagranite were first processed in a steel jaw crusher. An aliquot of about 30 g was powdered in an agate rind-disc mill. Rock powders were then dried at 105 °C for ca. 24 h. 200 mg of rock powder were mixed with 1.5 g of $LiBO_2$ flux in a graphite crucible. Subsequently, the crucible was placed in an oven and heated to 1050 °C for 15 min. The molten samples were dissolved in 5% HNO_3 (ACS grade nitric acid diluted in demineralised water). International reference samples (NCSDC71301, AGV-2 and W2A) and reagent blanks were added to the sample sequence, and analyzed together with the samples. For analyses of major elements, sample solutions were aspirated into an inductively coupled plasma emission spectrometry (ICP-ES) at the Geological Department of the Kocaeli university. The precisions of the major element concentrations were ≤3%, and the accuracies were ≤5% (2σ). For the determination of trace elements including rare earth elements, the solutions were aspirated into an inductively coupled plasma mass

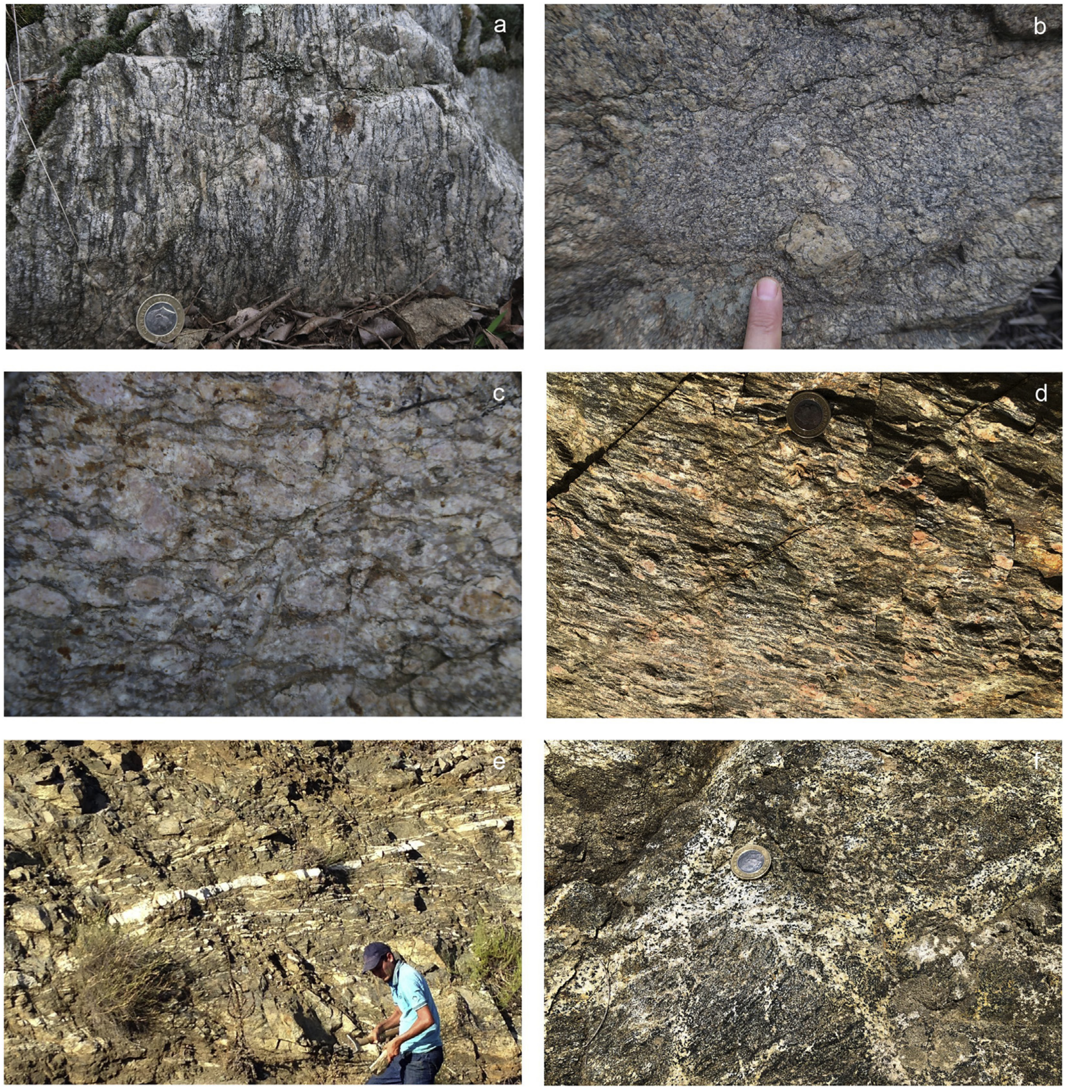

Fig. 4. Field pictures of the biotite-metagranite and amphibolite from the Sarıcakaya Massif. (a) Well-foliated biotite-metagranite. (b) Preserved large igneous K-feldspar grains, implying derivation from a porphyric granite. (c) Feldspar Augens in the biotite-metagranite, (d) Mylonitic fabric in the biotite-metagranite. (e) Foliated amphibolite cross-cut by several up to 20 cm-thick leucocratic sills/dykes. Note that the leucocratic veins are mostly foliation-parallel, but locally cross-cut the foliation. (f) Amphibolite with the diffuse hornblende-bearing leucosomes.

spectrometry mass spectrometer (Perkin-Elmer Elan DRC-e) at the Geochemical Laboratory of the Kocaeli University. Turkey. The precision and accuracy are ≤5% (2σ) for most elements as has been estimated from analyses of the standards AGV-2 and W-2A.

Mineral separation was performed at the Avrasya Yer Bilimleri Enstitüsü in Istanbul by conventional techniques involving breaking, sieving, washing, magnetic and heavy liquid separation. After the heavy liquid separation, the zircons were handpicked and placed on a double-sided band under binocular. After embedding into epoxy, the mount was polished to reveal the internal structures of the zircon and potential inclusions. The internal structures were revealed by cathodeluminescence imaging at the Jeoloji Mühendisliği Bölümü (Hacettepe) in Ankara. Apart from zircons from sample 10082, all U—Pb zircon dating were performed at the University of Gothenburg with an Agilent 8800 ICP-MS equipped with a New Wave NWR213 laser ablation system. The measurements were performed in a TV2 two-volume cell in helium atmosphere (0.7 l/min), with a laser spot size of 20 μm, a laser fluence of ca 6.2 J/cm^2 and a frequency of 10 Hz. The ablated sample aerosol is carried in He, and then mixed downstream with 4 ml N_2/min and 0.56 l Ar/min before reaching the ICP-MS. U—Pb dating of zircon were quantified using 91500 as primary standards. Data reduction was performed with help of URanos v. 2.06a (Dunkl et al., 2008; http://www.sediment.uni-goettingen.de/staff/dunkl/software/uranos.html). Secondary standards analyzed in the same run gave results as follows (^{206}Pb/^{238}U age, 2σ error, MSWD and number of analysis in brackets for results obtained in this study): Zircon GJ (598 $\pm$ 4 Ma, 0.4, 40) and Pl (344 $\pm$ 4 Ma, 0.69, 16). Zircon from the Kaap Valley Tonalite (KVT) gives ^{207}Pb/^{206}Pb ages of 3216 $\pm$ 25 Ma (MSWD of 0.55, $n = 5$). Compared to most recent literature data (Horstwood et al., 2016 for GJ-1 and PL, Schoene et al., 2006 for KVT), all ages agree within 2% to TIMS ages. Please note that all concordia ages are about 2%, and are therefore considered to be accurate within those age limits. Zircons from sample 10082 were dated by laser ablation split-stream inductively coupled plasma mass spectrometer (LASS-ICP-MS), using a Nu Plasma multicollector ICP-MS for U/Th-Pb data and an Agilent 7700 quadrupole ICP-MS for trace-element concentration at the Department of Earth Sciences, University of California (Santa Barbara), following the methods of Kylander-Clark et al. (2013). Samples were ablated using a Photon Machines Excite excimer laser system with a spot size of 25 μm, a repetition rate of 4 Hz and an approximate fluence of 1 J/cm^2. For this sample, data was processed with Iolite version 2.5 (Paton et al., 2011). Results for all zircons are plotted with IsoplotR (Vermeesch, 2018).

The in-situ Hf isotope data were acquired, using a 193 nm ArF laser connected to the Nu MC-ICP-MS. Ablation was conducted in He (flow rate ~0.95 l/min) and combined with argon (~0.9 l/min), using a spot size of 40 μm and a 5 Hz laser pulse repetition rate over a 60 s ablation period. The most critical factor in obtaining accurate $^{176}Hf/^{177}Hf$ ratios by laser ablation concerns the ability to correct for the isobaric interference of Lu and Yb on ^{176}Hf, depending on the REE content of the analyzed zircon. The correction itself is performed by measuring an interference-free Yb isotope during the analysis, such as ^{171}Yb or ^{173}Yb, and then calculating the magnitude of the ^{176}Yb interference by using the recommended $^{176}Yb/^{171}Yb$ or $^{176}Yb/^{173}Yb$ ratios of Segal et al. (2003). The Lu correction is performed in the same fashion by monitoring ^{175}Lu and using $^{176}Lu/^{175}Lu = 0.02669$. To control and correct the measured Hf-ratios, we analyzed two zircon standards with different REE contents (Monastery, Temora and Mud Tank). For the calculation of the ε-Hf values, the following present-day ratios of the Chondritic Uniform Reservoir (CHUR) were used: $(^{176}Hf/^{177}Hf)_{CH} = 0.282769$ (Nowell et al., 1998) and $(^{176}Lu/^{177}Hf)_{CH} = 0.0334$.

5. Petrography

The biotite-metagranite is characterized by medium to coarse grain sizes (0.12–5 mm), and display blastomylonic to mylonitic textures (Figs. 4a–d and 5a, b). It contains perthitic microcline, plagioclase, quartz, biotite and ± muscovite. Accessory minerals are apatite and zircon. Secondary minerals are muscovite, calcite, albite and rare epidote. Microperthitic microcline and plagioclase locally form porphyroclasts with inclusions of quartz, which are set in a matrix consisting of recrystallized feldspar and quartz and biotite (Fig. 5b). With decreasing biotite content, the metagranite grades into felsic types. Quartz locally forms ribbons, or statically recrystallized grains, while feldspars form both porphyroclasts and small deformed grains. Such deformational features suggest that mylonitic foliation has developed under low- to medium-grade metamorphic conditions (see Passchier and Trouw, 2005, pp. 61–63).

The amphibolite is well foliated, fine to medium grained (0.2–2 mm), and devoid of any relict igneous texture (Fig. 5c, d). Mineral constituents are hornblende, plagioclase ($An_{26–39}$), and ilmenite, and minor amounts of titanite, biotite and quartz. Accessory minerals are zircon and apatite. Amounts of titanite, biotite and quartz are variable. With increasing modal amounts of quartz, amphibolite grades into quartz amphibolite. Biotite is locally intergrown with hornblende. Hornblende is characterized by subidioblastic grains with local inclusions of plagioclase, ilmenite and minor quartz. Plagioclase is locally bent, and displays undulose extinction. Ilmenite is mostly surrounded by titanite. Amphibolite is variably overprinted by the subgreenschist to greenschist-facies mineral assemblages involving chlorite, albite, K-feldspar, pumpellyite, epidote, titanite, actinolite and calcite. In the hydrothermally overprinted

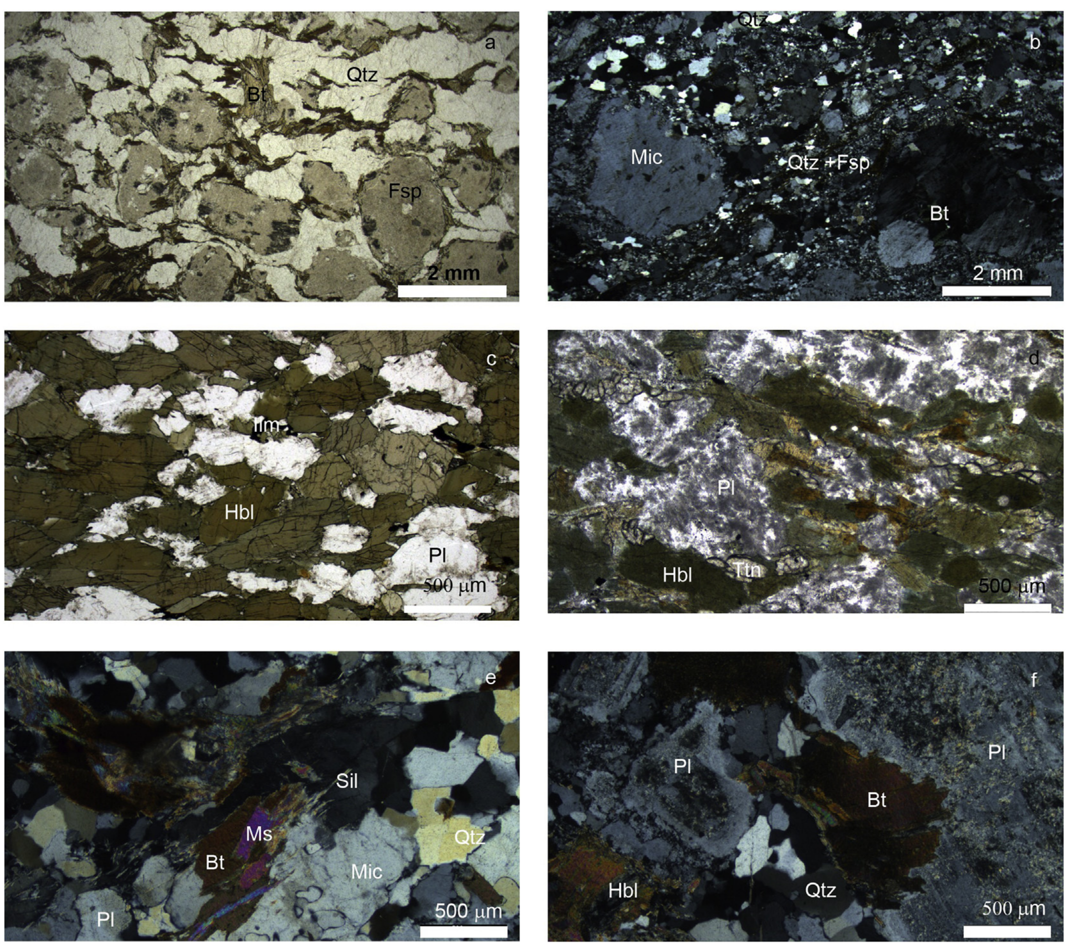

Fig. 5. Thin section micrographs showing textural features of the biotite-metagranite, amphibolite, two-mica metagranite and hornblende-biotite metatonalite. (a) Augen-gneissic texture in biotite-metagranite. Augens are represented by feldspar grains (Fsp), and matrix by recrystallized flattened quartz (Qtz) and recrystallized biotite (Bt). (b) Feldspar porphyroclasts (Fsp) in a biotite-metagranite. Matrix consists of recrystallized quartz (Qtz) and feldspars (Fsp). (c) Hornblende (Hbl) and plagioclase (Pl) grains in a well-foliated amphibolite. Opaque minerals are ilmenite (Ilm). (d) Amphibolite consisting of hornblende (Hbl), plagioclase (Pl) and titanite (Ttn). Plagioclase displays a cloudy color, due to fine-grained intergrowths of albite, epidote, pumpellyite and ± quartz. (e) Intergrowths of biotite (Bt) and muscovite (Ms) in a two-mica granite. Note that fibrolite grows along the tips of muscovite. (f) Well-preserved igneous texture in the hornblende-biotite metatonalite. Quartz (Qtz) forms interstitial grains next two euhedral plagioclase grains (Pl). Biotite is the dominant mineral, and hornblende form islets in the biotite.

samples, plagioclase display a cloudy color caused by fine grained intergrowth of albite with pumpellyite and epidote (Fig. 5d). There are also late up to 2 mm-thick veinlets of albite and calcite.

6. U—Pb zircon dating

In order to constrain the igneous crystallization ages of the metaigenous rocks within the Sarıcakaya Massif, laser ablation inductively coupled plasma mass spectrometry (LA-ICP-MS) zircon dating has been performed on seven samples (54A, 64B, 138A, 161A, 188A, 188B and 10082). Coordinates of the dated samples are given in Table A1, and their locations are shown in Fig. 3. Samples 54 and 188A are from amphibolite, samples 64B and 138A are from biotite-metagranite. Sample 188B is from a felsic dike within the amphibolite. Samples 161A and 10082 are not part of the metagranite-amphibolite complex (Fig. 3), and described petrographically in detail below. Sample 161A is a medium-grained two-mica metagranite comprising biotite, muscovite, microcline, plagioclase and sillimanite (Fig. 5e). Apatite, zircon and monazite are accessory minerals. Former micrographic textures and myrmekites are well-preserved. Sillimanite grows at the expense of igneous muscovite. Sample 10082 is a medium to coarse-grained hornblende-biotite metatonalite with granular to porphyritic texture from the Bozöyük area (Fig. 3a), and comprises biotite, plagioclase, quartz and hornblende (Fig. 5f). Accessory minerals are ilmenite, zircon and apatite. The coarse foliation is defined by metamorphic fine-grained biotites which have grown at the expense of the large igneous biotite. Kink bands and undulose extinction in igneous biotite are common. Secondary minerals are calcite, titanite, epidote and albite.

Fig. 6 shows the cathodo-luminescence images of the zircons from the different samples. Overall, zircons from the amphibolite samples (54A and 188A) are prismatic, and show well-developed oscillatory and locally sector zoning. Obvious inherited cores are locally present, and confined mainly to samples 188B and 161A, felsic dike within amphibolite and sillimanite-bearing two mica metagranite, respectively. Inclusions of silicate minerals (e.g. quartz, feldspars, biotite and hornblende) and apatite are common. Zircons from the biotite-metagranite have dark luminescent internal domains overgrown by brighter margins. All the dated zircons are characterized by strongly fractionated rare earth element patterns with pronounced negative Eu anomaly and positive Ce anomaly (figures in Table A1). The U and Th concentrations of the zircons are in the range 129–350 and 24–190 μg/g, respectively, resulting in Th/U ratios of 0.23–0.54 (Table A1). Only the zircons from sample 188B (felsic dike within amphibolite) have very low Th/U ratios of 0.07–0.32. Presence of minute inclusions and metamictized domains leads to elevated concentrations of Al, P, Ca and La as well as the disappearance of positive Ce and negative Eu anomalies. Such analyses were disregarded in the age calculations. Also, the analysis with ablation times ≤45 s are mostly regarded as poor analysis. All these textural and geochemical characteristics point to growth of zircon from a melt phase rather than metamorphic growth. Geochemical features of the zircons from sample 188B are consistent from the crystallization from the low-temperature partial melts from the local sources. Metamorphic overgrowth on the igneous grains are either non-existent or very thin (≤10 μm). Zircon age results from different metaigneous rocks are given separately below.

6.1. Amphibolite and biotite-metagranite

After screening the fourteen analysis on the zircon grains from sample 54A (amphibolite), ten zircon grains yield a concordia age of 418.75 ± 6.50 Ma (all errors are reported as 2σ; MSWD = 0.48) (Fig. 7a). One zircon grain (# 10) gives a substantially older $^{206}Pb/^{238}U$ age of 468 ± 5.4 Ma, interpreted as an inherited grain (Table A1). Out of the 13 measurements on the zircons from the amphibolite sample 188A (amphibolite), ten zircon grains yielded a concordia age of 434.05 ± 6.81 Ma (MSWD = 0.7) (Fig. 7b). Out of 16 measurements on zircon grains from the biotite-metagranite 64B, only three zircon

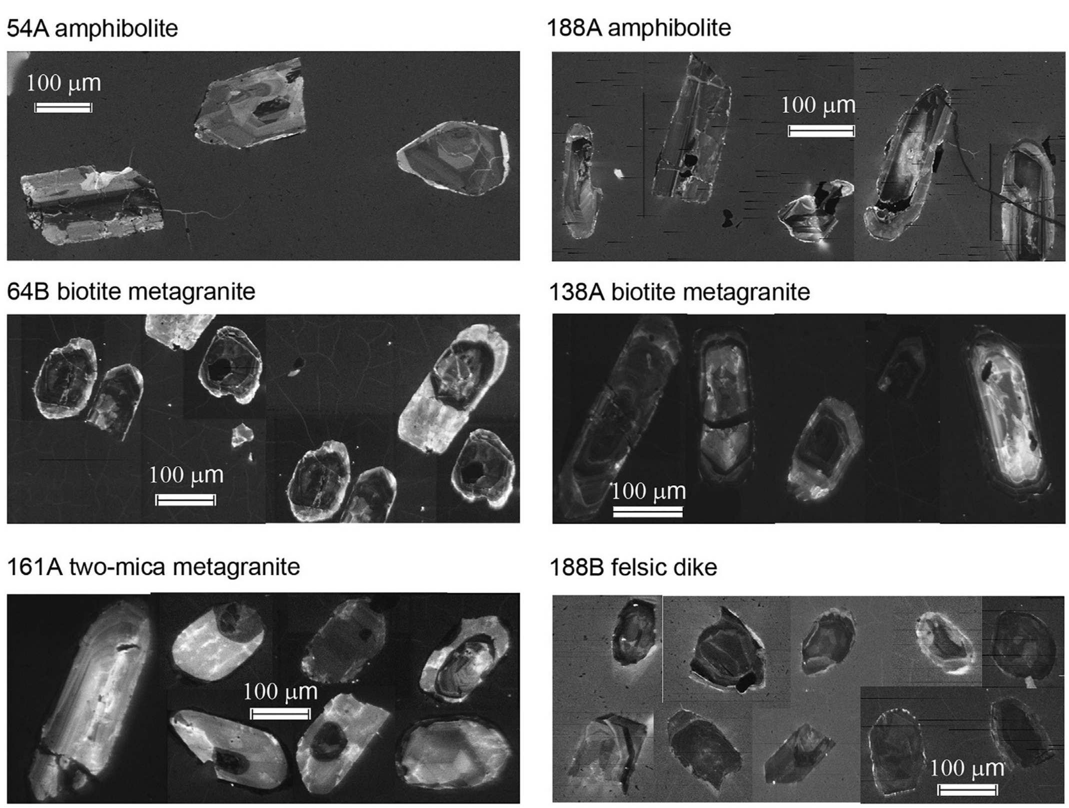

Fig. 6. Cathodo-luminescence (CL) images of the dated zircons from the Sarıcakaya Massif (NW Turkey).

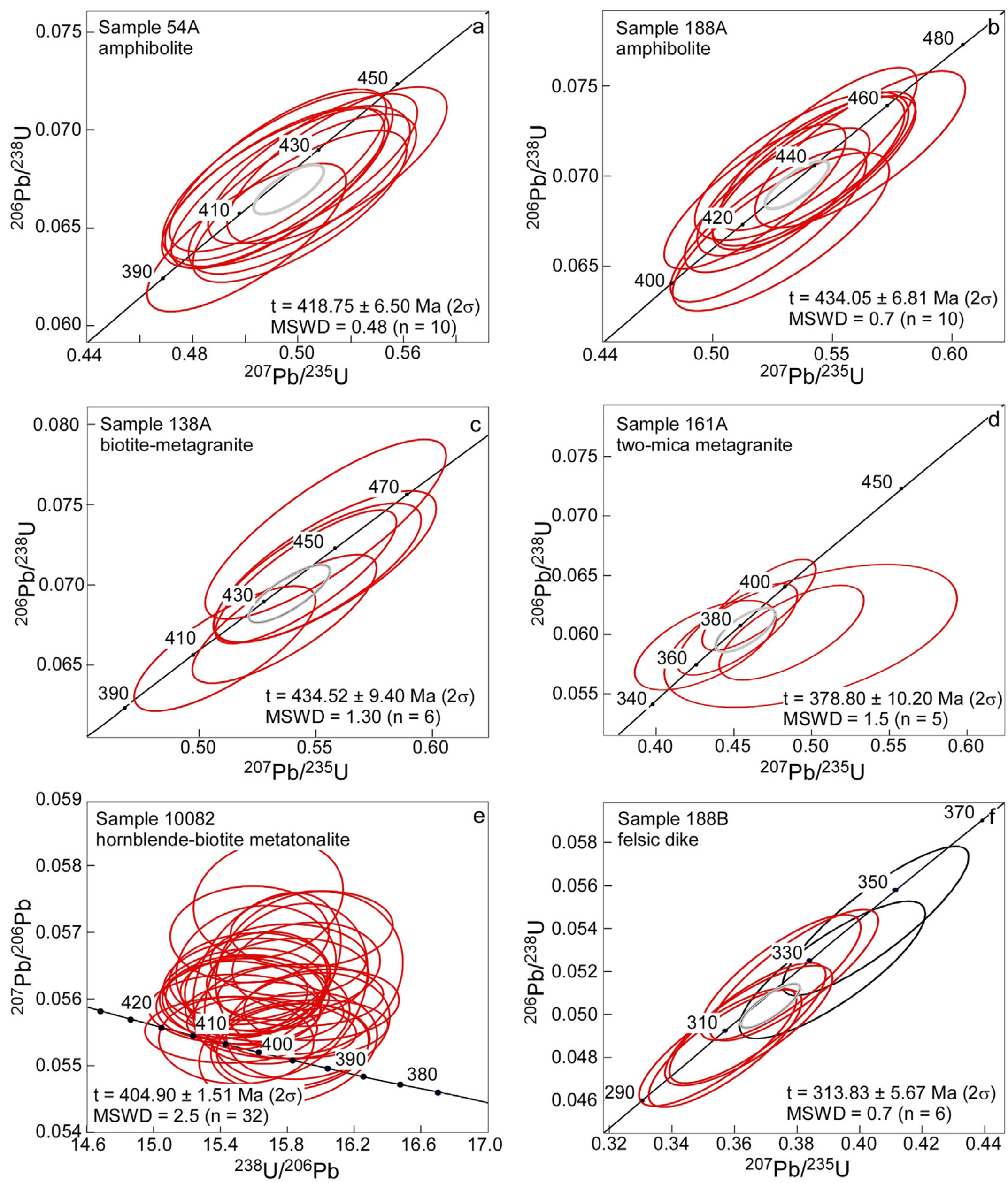

Fig. 7. U—Pb concordia diagrams showing LA-ICP-MS zircon data for the different samples from the Sarıcakaya Massif (Eskişehir). Error ellipses are given at 2σ level. Ages were calculated by IsoplotR (Vermeesch, 2018).

grains define a poor concordia age of 430.09 ± 16.04 Ma (MSWD = 1.5) (Fig. A1). All the dated grains display elevated concentrations of Al (208–5735 μg/g), Ca (304–5642 μg/g), P (125–16,177 μg/g), Ti (2.9–1189 μg/g) and La (7–282 μg/g). Furthermore, their rare earth element patterns are characterized by steadily increasing shape from La to Lu, whereby the anomalies of Ce and Eu are almost not recognizable (Table A1). Only the rare earth element patterns of the concordant analysis display pronounced positive Ce and negative Eu anomalies. The cathodo-luminescence images of the dated zircon grains are characterized by a dark-looking cores overgrown by bright rims (see 64B in Fig. 6). We ascribe elevated concentrations of Al, Ca, P and Ti to metamictization together with the presence of the common minute inclusions. Out of thirteen measurements on the zircon grains from sample 134A (biotite-metagranite), six grains define a concordia age of 434.52 ± 9.40 Ma (MSWD = 1.3) (Fig. 7c). Only one grain (#8) yielded a $^{206}Pb/^{238}U$ age of 603 ± 4.8 Ma, interpreted as an inherited grain.

All these age values from the amphibolite and biotite-metagranite suggest that the protoliths of the amphibolite and biotite-metagranite have Silurian igneous crystallization ages.

6.2. Two-mica metagranite and hornblende-biotite metatonalite

Out of 16 measurements on zircons from two-mica metagranite (sample 161A), five zircon grains define a concordia age of 378.80 ± 10.20 Ma (MSWD = 1.5) (Middle to Late Devonian) (Fig. 7d). Additionally, the sample contains inherited zircon grains: Three grains yield a concordia age of 563.75 ± 18.77 (MSWD = 0.87) (Fig. A1). The other inherited zircons have $^{206}Pb/^{238}U$ ages of 1084 ± 23, 1951 ± 4, 2052 ± 5 and 2075 ± 4.6 Ma (Table A1). Thirty-two measurements have been carried out on the zircon grains from the metatonalite sample (10082). The data points are slightly discordant, yielding a concordia age of 404.90 ± 1.51 Ma (MSWD = 2.5) (Early Devonian) on the Tera-Wasserburg plot (Fig. 7e). With the common lead correction after Stacy-Kramers, the concordia age becomes 397.26 ± 1.57 Ma (MSWD = 0.53).

On the basis of the textural and geochemical features of the zircons, the age values are interpreted as the protolith ages of the two-mica metagranite and metatonalite. This situation suggests that the Sarıcakaya Massif also includes metaigneous rocks with Devonian ages in addition to those with the Silurian ages.

6.3. Felsic dike

Seven zircon grains from sample 188B (felsic vein in amphibolite) gave a concordia age of 318.23 ± 5.46 Ma (MSWD = 1.6, $n = 8$). Seeing that the age population with the oldest data grains are excluded on the basis that they might represent mixed analysis, the obtained age becomes 313.83 ± 5.67 Ma (2 s, MSWD = 0.7; $n = 6$) (Fig. 7f). This zircon population is characterized by low concentrations of Ti (1.5–3.1 μg/g) and Th/U ratios of 0.07–0.23 (Table A1). In addition to this zircon population, there are two inherited zircon grains with $^{206}Pb/^{238}U$ ages of 385 ± 5.6 and 445 ± 5.4 Ma. The age value 313.83 ± 5.67 Ma (Late Carboniferous) is interpreted as the igneous crystallization age of the felsic dike.

To summarize, the zircon age data show that the igneous crystallization ages of the distinct metaigneous rocks in the Sarıcakaya Massif range from 432.57 ± 6.44 to 378.56 ± 6.21 Ma (Silurian to Late Devonian), and the ages of the *syn-* to post-metamorphic intrusions are 331–310 Ma (Early to Late Carboniferous) (Ustaömer et al., 2012b; our unpublished data).

7. Whole rock geochemistry

A total of twelve samples from biotite-metagranite and amphibolite with Silurian igneous crystallization ages were analyzed for their major and trace element compositions. The major- and trace-element compositions together with the UTM coordinates are listed in Table A2. Both the biotite-metagranite and amphibolite display cm- to dm-scale heterogeneities in the outcrop, which include porphyroblasts and porphyroclasts in the biotite-metagranite and irregular leucosomes (Fig. 4a–f), therefore special care was taken during sampling to get representative samples. Fresh samples with a weight of ca. 5 kg were taken away from any visible leucosomes, dikes and veins. Any weathering crust was removed in the field. Seeing that both the amphibolite and biotite-metagranite were subjected to upper amphibolite-facies metamorphism with local developments of leucosomes and subsequently to subgreenschist-facies overprint (Fig. 5d), the effects of metamorphism on element mobility are important. The high-field strength elements (Th, Nb, Ta, Zr, Hf and Ti), rare earth elements (REE) and transition metals (Co, Sc, V, Cr and Ni) are commonly regarded as immobile during metamorphism and hydrothermal events (Pearce, 2014; Polat et al., 2003). We therefore base our interpretations specifically on high-field strength elements and rare earth elements and their ratios. Relative immobility of rare earth elements including Th and Nb is implied by the parallel shape of the bulk-silicate earth normalized rare earth element patterns of the investigated samples (Fig. 8).

The biotite-metagranites display relatively fractionated, spoon-shaped concave-upward rare earth element patterns (La_N/Yb_N = 9–13) with significant negative anomalies of Nb and Eu anomalies (Eu/Eu^* = 0.38–0.40) on the bulk silicate earth normalized rare earth element patterns including Th and Nb (Fig. 8a). A noteworthy feature is that middle rare earth elements are nearly unfractionated relative to the heavy ones (Tb_N/Yb_N = 1.47–1.54), ruling out significant amount of residual garnet in the source and during magmatic fractionation. On a Nb/Y vs Zr/Ti variation diagram, the biotite-metagranite plots into fields of the trachyte and trachy andesite (Fig. 9a).

The amphibolites display quite variable Mg numbers (= molecular MgO/(MgO + FeO_{tot})*100) are, ranging from 53 to 92 (Table A2). Samples with high Mg numbers (86–92), also display elevated Cr concentrations (172–379 μg/g). The elevated Mg numbers are most probably

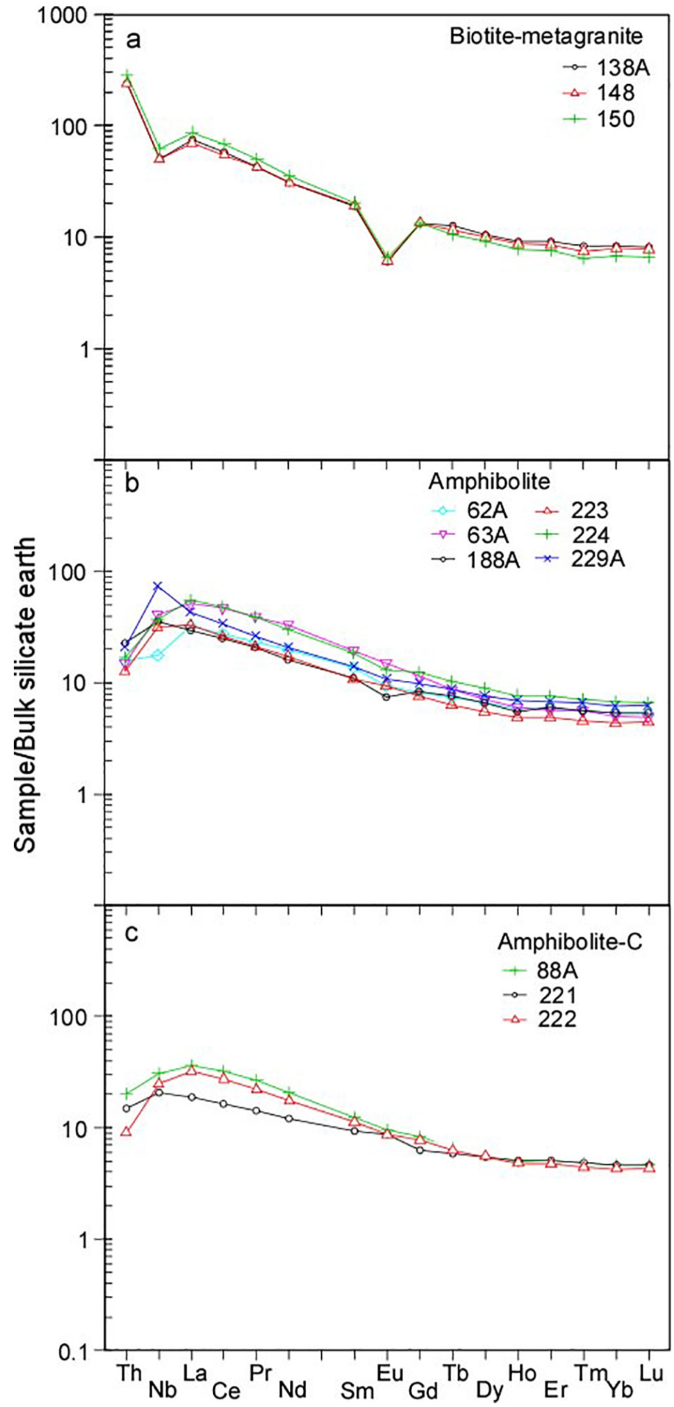

Fig. 8. Bulk Silicate Earth (BSE; synonymous with a primitive or primordial mantle) rare earth element patterns including Nb and Th. Bulk silicate earth concentrations are taken from Palme and O'Neill (2014). (a) Biotite-metagranite, (b) Amphibolite, (c) Amphibolite-C (cumulate).

caused by mineral accumulation (e.g., pyroxene) and are not a primary magmatic feature. Consequently, the amphibolites with high Mg numbers are interpreted to have derived from former pyroxene cumulates. The amphibolites with Mg numbers between 53 and 70 were probably derived from the slightly fractionated mantle melts. On the bulk silicate earth normalized rare earth element patterns including Th and Nb (Fig. 8b), the amphibolites are characterized by slightly fractionated rare earth patterns (La_N/Yb_N = 6–10), whereby the middle rare earth elements are slightly fractionated relative to heavy ones (Tb_N/Yb_N = 1.27–1.73), ruling out the presence of residual garnet in the source.

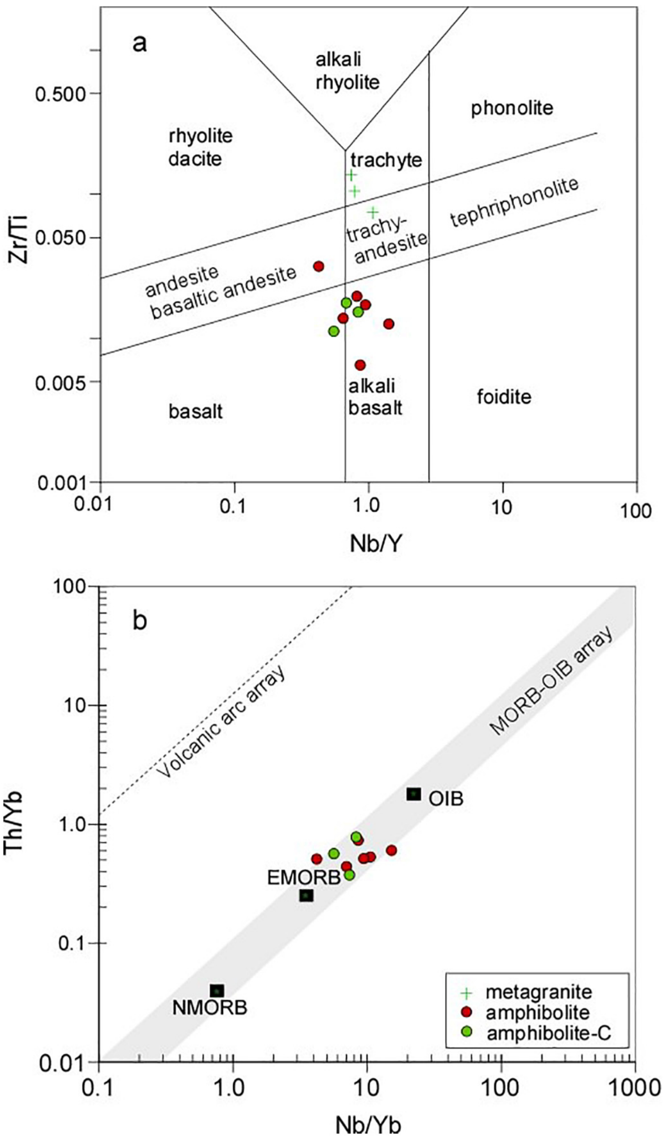

Fig. 9. (a) Nb/Y vs Zr/Ti classification diagram (Pearce, 1996) showing subalkaline and alkali basalt affinities of amphibolite samples from the Sarıcakaya Massif. (b) Data of the amphibolite plotted in the Nb/Yb vs Th/Yb diagram (Pearce, 2008).

A consistent negative Nb anomaly is absent. On the rare earth diagrams, the samples display a weak to absent Eu amomaly (Eu/Eu* = 0.77–1.03), suggesting insignificant plagioclase fractionation. In the Nb/Y vs Zr/Ti diagram of Pearce (1996), the amphibolites plot in the fields of alkali basalt and subalkali basalt and andesitic basalt (Fig. 9a). In the Nb/Yb vs Th/Yb diagram of Pearce (2008; Fig. 9b), the amphibolites plot in the upper MORB-OIB array, and lack a marked sedimentary subduction component, which is in line with the rare earth element pattern including Th and Nb of the metagabbros which do not show any marked Nb anomaly. The amphibolites with cumulate affinities display rare earth element patterns (Fig. 8c) comparable with the amphibolites, and plot on the MORB-OIB array on the Nb/Yb and Th/Yb diagram (Fig. 9a, b).

To summarize, the biotite-metagranite is derived from high-K to shoshonitic quartz monzonite to granite, and the amphibolite from anorogenic transitional tholeiitic to alkaline gabbroic rocks.

8. Hafnium isotopes in zircon

Hafnium isotopic compositions of zircon grains have been measured on the dated zircons of Silurian crystallization age from two amphibolite (54A, 188A) and two biotite-metagranite samples (64B, 138A). Totally twenty-two grains of zircon were analyzed for hafnium isotopic composition. The analytical data are listed in Table A3. Twenty-two analyses of Mud Tank zircon and twelve analyses of Temora zircon during measurement session yielded average $^{176}Hf/^{177}Hf$ values of 0.282544 ± 0.000008 and 0.282696 ± 0.000012, respectively.

Overall, the initial εHf values of the zircons, calculated to 440 Ma, display wide intersample variations from −26 to 12 (Fig. 10). The amphibolite zircons are characterized entirely by positive initial εHf values (0.90–12.44), and the biotite-metagranite zircons entirely by negative initial εHf values (−5 to −21). Furthermore, there are noticeable differences in the initial εHf values of zircons from different amphibolite and biotite-metagranite samples. The initial εHf values of the igneous zircons in amphibolite sample 54A range from 2.88 to 12.44 with a medium of 6.42 ± 2.21 (2σ), and those in amphibolite sample 188A from 0.90 to 6.21 with a medium of 2.95 ± 1.62 (2σ) (Fig. 10a, b). In clear contrast to the igneous zircons in the amphibolites, the initial εHf values of the igneous zircons in sample 64B range from −5.01 to −15.42 with a medial value of −9.01 ± 2.19 (2σ). The igneous zircons in biotite-metagranite sample 138A display initial εHf values ranging from −12.34 to −26.04 with a medial of −16.02 ± 2.91 (2σ). Strongly negative initial εHf values are related to the inherited zircon grains. The Hf isotope model ages range from 0.94 to 1.17 Ga in amphibolites and from 1.48 ± 0.49 to 1.77 ± 0.67 Ga in biotite-metagranite (Table A3).

The zircon Hf isotope data conclusively indicate that the protoliths of the amphibolite were derived from juvenile melts of heterogeneously depleted mantle source, and those of the biotite-metagranite, on the other hand, from the crustal sources.

9. Discussion

9.1. Protolith age range of the upper amphibolite-facies metamorphic rocks

Recent incremental Ar—Ar mica ages suggest that the upper amphibolite-facies metamorphism in the Sarıcakaya Massif occurred during Early Carboniferous (Uğurcan et al., 2019). This age closely agrees with the age of felsic dike (sample 188B, at 319.46 ± 4.76 Ma) and the ages of the non-metamorphic intrusive rocks within the massif, ranging from 327.2 ± 2 to 309 ± 5 Ma (Visean to Moscovian, Early to Late Carboniferous) (Ustaömer et al., 2012b, this study). Thus, the Sarıcakaya Massif represents the equivalent of the Early Carboniferous high-T/middle to low-pressure metamorphic rocks in the Dzirula, Yusufeli, Kurtoğlu and Pulur massif in the eastern part of the Sakarya Zone (Fig. 1) (Mayringer et al., 2011; Topuz et al., 2004a, 2007; Topuz and Altherr, 2004; Ustaömer et al., 2012a).

Detrital zircons in the metaclastic rocks have age spectra of 503–1041 and 1600–2200 and 2500–2700 Ma (Ustaömer et al., 2012b; own data). The protoliths of the metaclastic rocks were probably deposited during Late Cambrian-Ordovician time, as deduced from the age of the youngest detrital zircon grain (503 ± 6 Ma) and by Silurian (ca 440–420 Ma) and Devonian (ca 400–380 Ma) magmatic rocks, which intrude the metaclastic sequence. This interpretation is in line with the suggestion by Ustaömer et al. (2012b) on the basis of the resemblance of the detrital zircon age spectra of the metaclastic rocks to those of the Cambrian-Ordovician clastic rocks in Jordan (Gondwana). Thus, the Sarıcakaya Massif includes igneous and sedimentary rocks ranging in age from Cambrian to Middle Devonian. A noteworthy feature of the Sarıcakaya Massif is that the Devonian granitic rocks are were involved in the Early Carboniferous regional metamorphism. So far, Early to Middle Devonian granites were described from locations whey they intrude phyllites of unknown age.

9.2. Tectonic setting of Silurian acidic to basic magmatism

The U—Pb zircon age data unambiguously indicate that the biotite-metagranite and amphibolite within the Sarıcakaya Massif were derived

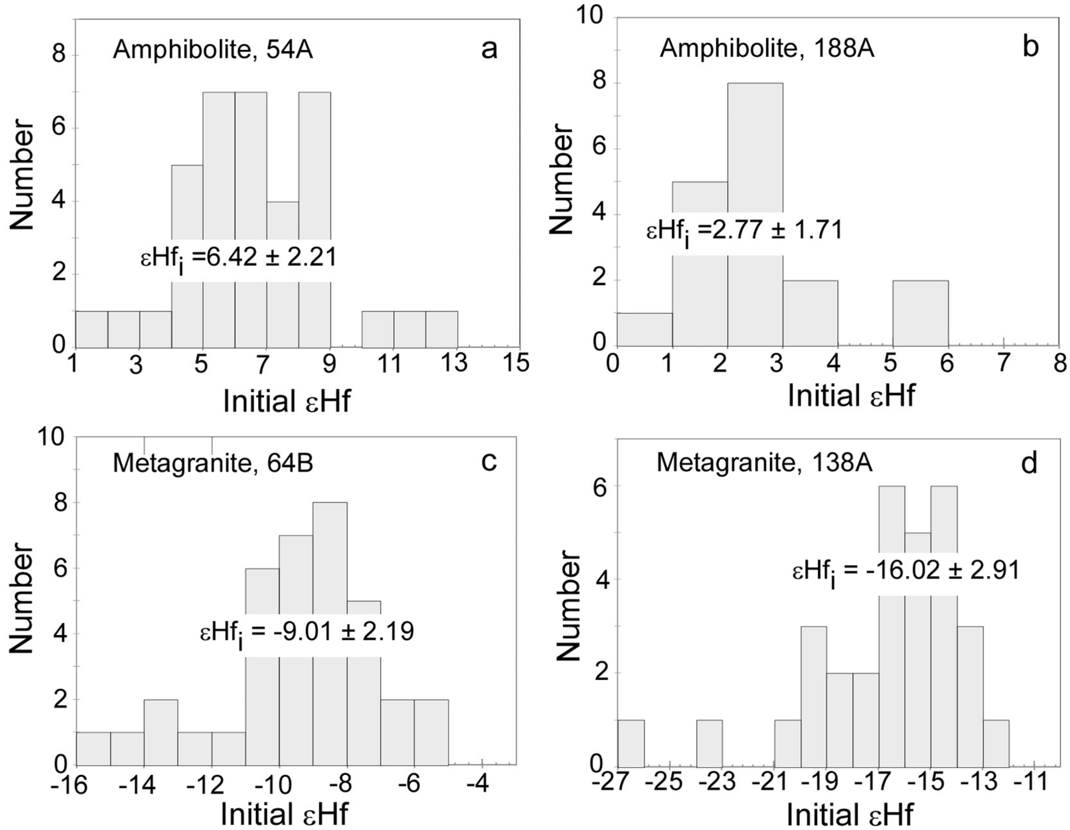

Fig. 10. Histograms showing initial εHf values of the igneous zircons in the amphibolite and biotite-metagranite from the Sarıcakaya Massif.

from former Silurian granite and gabbro. No accretionary complex of Silurian age is known in the Sakarya Zone and its eastern and western elongations so far. Hence, we will discuss the tectonic setting of the Silurian magmatism solely based on its geochemical characteristics.

The Hf isotopes of zircons suggest that the protoliths of amphibolite were derived from the juvenile mantle melts, and those of the biotite-metagranite were mainly products of the anataxis of the preexisting crustal material. Thus, geochemical features of the amphibolite are of special importance to constrain the geodynamic setting of the magmatic protoliths. The amphibolite displays transitional tholeiitic to alkaline signatures, and is devoid of a marked sedimentary subduction component, as deduced by the absence of a noticeable negative Nb anomaly and their position on the MORB-OIB array in the Nb/Yb vs Th/Yb diagram (Figs. 8b and 9b). Formation in a subduction-unrelated setting is also inferred from other geochemical discrimination diagrams such as (i) Zr vs Zr/Y diagram of Pearce and Norry, 1979, and (ii) Ti vs V diagram after Shervais (1982) (not shown). On a Zr versus Zr/Y diagram, all amphibolite samples plot in the field of within-plate basalts. The Ti/V ratios, which is a proxy for the oxygen fugacity and presence of hydrous fluids in the mantle, are between 20 and 50, falling into the field defined by continental flood, back arc and ocean floor basalts. On the other hand, subduction-related rocks are characterized by Ti/V ratios <20 (Shervais, 1982). To sum up, the Silurian basic to acidic magmatism formed in a subduction-unrelated rift-related setting (see below for further discussion).

9.3. Geodynamic implications of the Silurian basic and acidic magmatism

The biotite-metagranite and amphibolite with Silurian igneous crystallization ages represent the first record of Silurian magmatism in the Sakarya Zone. Several provenance studies on the metaclastic rocks of the Sakarya Zone in the literature report presence of the Silurian detrital zircons; these include (i) metaclastic rocks around the Devonian granites in the western part of the Sakarya Zone (Aysal et al., 2012b), (ii) Carboniferous low-grade metaclastic rocks from the Yusufeli Massif in the eastern part of the Sakarya Zone (Ustaömer et al., 2012a), (iii) metaclastic rocks within the Permo-Triassic accretionary complexes in the western Pontides (Ustaömer et al., 2016), and (iv) metaclastic rocks in the Strandja Massif, (Sunal et al., 2008). However, the abundance of Silurian detrital zircons is subordinate to the Devonian and Carboniferous detrital zircons. We, therefore, infer that Silurian magmatism must be common in the Sakarya Zone, but volumetrically less than Devonian and Carboniferous magmatism.

Silurian basic to acidic magmatism is also sporadically documented in the eastern and western elongations of the Sakarya Zone, for example Armorica in the European Variscides, partly involved in Alpine Orogeny (e.g., Antić et al., 2016; Casas et al., 2010; Cliff, 1980; Dombrowski et al., 1995; Himmerkus et al., 2009; Putiš et al., 2009; Reischmann and Anthes, 1996; Rubatto et al., 2001; Somin, 2011) (see filled diamonds in Fig. 1). Only a limited number of studies presented whole-rock chemical analyses on these rocks. Currently, there is no consensus on the tectonic setting of the Silurian magmatism. The proposed tectonic settings range from compressional magmatic arc to crustal extension leading to rifting. Antić et al. (2016) describe 439 ± 2 Ma felsic rocks with within-plate geochemical affinities from the Serbo-Macedonian Massif. Furthermore, Schulz et al. (2004) describe 430 Ma old metabasic rocks with alkaline within-plate affinities in the Austroalpine basement, and relate it to the Paleo-Tethyan passive margin along the north Gondwana periphery.

As stated earlier, the geochemical features of the amphibolite suggest formation in a subduction-unrelated setting. We cautiously interpret these acidic to basic magmatism to have formed in a rift-related setting. Timing of the detachment of the Sakarya Zone from the northern margin of Gondwana, which led to the opening of the Paleo-Tethys, is not well-constrained (e.g. Stampfli and Borel, 2002; von Raumer et al., 2013). The metaclastic rocks in the Sarıcakaya Massif have identical detrital zircon age spectra with those of Cambrian–

Ordovician sandstones along the northern periphery of the Arabian platform in Jordan (Ustaömer et al., 2012b). This can be interpreted that the Sakarya Zone was still part of Gondwana during Cambrian-Early Ordovician times. On the other hand, the oldest deep-sea sedimentary blocks within the Paleo-Tethyan accretionary complexes are of Late Silurian (Kozur, 1998) and Devonian ages (Okay et al., 2011), indicating that the Paleo-Tethys was open during Late Silurian time. The Anatolide-Tauride Block, which detached from Gondwana during Early Triassic (Akal et al., 2012; Göncüoğlu et al., 2003; Şengör and Yılmaz, 1981; Uzunçimen et al., 2011) locally includes anorogenic A-type metagranites of Middle Ordovician to Silurian igneous crystallization ages (430–465 Ma) (Okay et al., 2008a; Özbey et al., 2013; Topuz et al., under preparation) (Fig. 1). They were interpreted to have formed in a rift environment along the northern margin of Gondwana during the Ordovician. On the basis of such evidence, we ascribe the Silurian anorogenic acidic to basic magmatism to a continental rifting event leading to the detachment of Armorica from the northern margin of Gondwana, and opening of the Paleo-Tethyan oceanic realm during Late

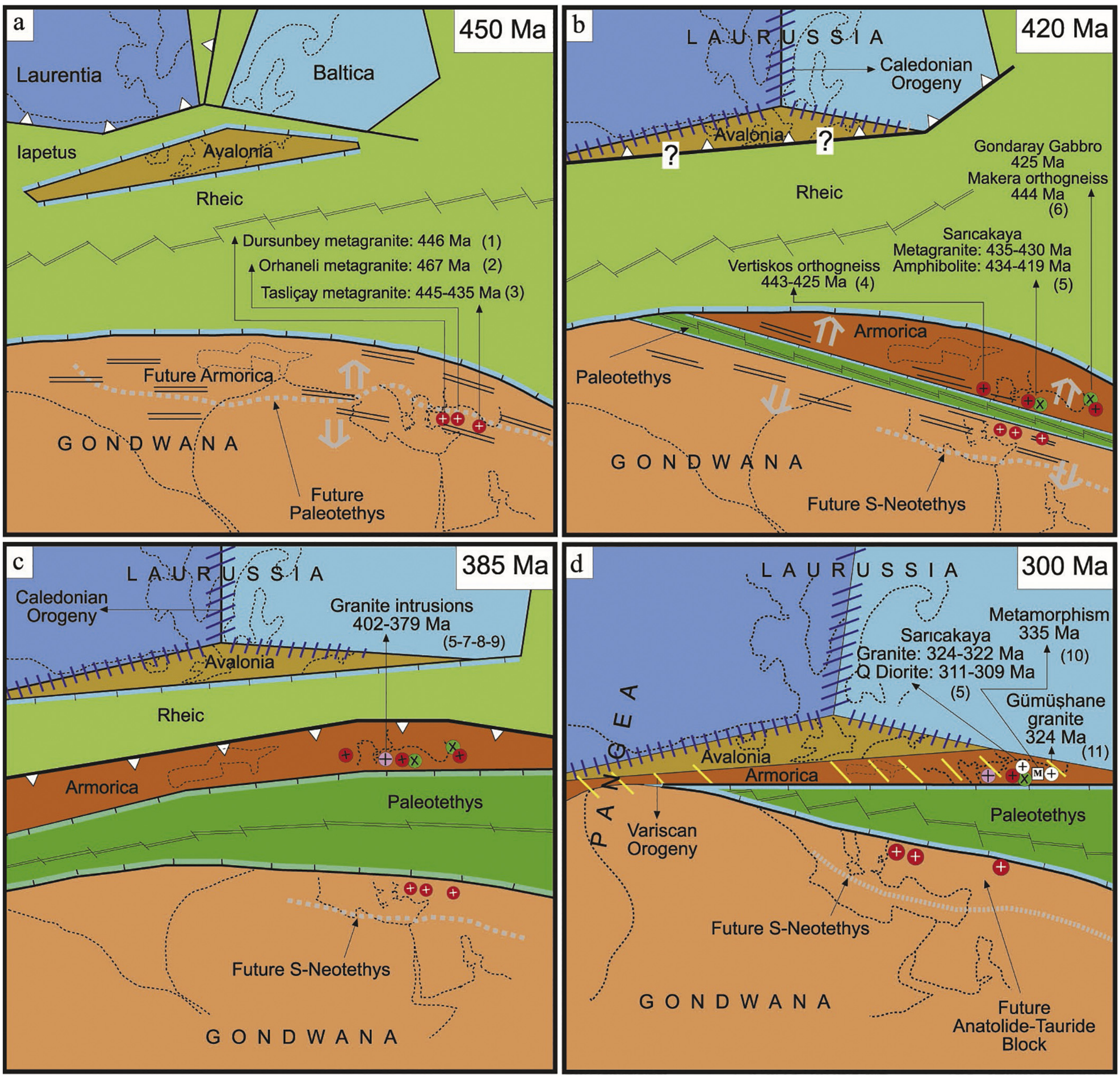

Fig. 11. Suggested evolutionary model for the anorogenic basic to acidic magmatism in the Sarıcakaya Massif. (a) During the Late Ordovician, northern margin of the Gondwana was undergoing extension. This extension led to the development of several, locally A-type, granites. To the north of the Rheic Ocean, Laurentia, Baltica and Avalonia were not assembled yet. The vergence of subduction leading to the closure of the Iapetus Ocean was taken from Nance and Linnemann (2008). (b) During Silurian, Armorica, thus the Sakarya Zone, was detached from the northern margin of Gondana, leading to the opening of Paleo-Tethys. Contemporaneous with the opening, basic and acidic magmatism developed. The Laurentia, Baltica and Avalonia were assembled to Laurussia. Subduction beneath Laurussia is taken from Stampfli et al., 2013. (c) During Devonian, the Sakarya Zone was the site of voluminous granitic magmatism, probably due to the southward subduction of the Rheic Ocean which was probably initiated during Early Devonian. (d) By the Late Carboniferous, the Sakarya Zone (Armorica) collided with Laurussia, leading to the Variscan Orogeny. Consequently, a LP-HT metamorphism associated with voluminous granite and gabbro intrusions developed. References: [1]Özbey et al. (2013), [2]Okay et al. (2008a), [3]Topuz et al. (under preparation), [4]Himmerkus et al. (2009), [5]This study, [6]Somin (2011), [7]Okay et al. (1996), [8]Aysal et al., 2012a, [9]Sunal (2013), [10]Topuz et al. (2004a), and [11]Topuz et al. (2010).

Ordovician-Silurian times. This interpretation is in line with the suggestions of Stampfli and Borel (2002), Schulz et al. (2004), von Raumer and Stampfli (2008) and von Raumer et al. (2013) that the Paleo-Tethys opened during the Late Ordovician-Silurian. Commonly, the paleogeographic reconstructions suggest the opening of the Paleo-Tethys as a back-arc ocean (e.g. Stampfli and Borel, 2002; von Raumer et al., 2013; von Raumer and Stampfli, 2008). However, the available geochemical data from Sarıcakaya and Serbo-Macedonian massifs and Austroalpine basement do not provide any evidence for a back-arc origin. Rifting along the northern margin could have been facilitated by a subduction beneath Laurussia or a plume at the northern margin of Gondwana.

On the basis of the above-stated constraints, we suggest the following evolutionary model (Fig. 11). During Ordovician, the Rheic Ocean had reached its widest dimension, and the Sakarya Zone, thus Armorica, was still part of Gondwana. During the Middle Ordovician to Silurian, the northern margin of Gondwana was undergoing extension. This event was associated with the formation of several anorogenic basic to acidic igneous rocks on the northern margin of Gondwana (Fig. 11a). During the Late Silurian, Armorica was already detached from Gondwana, and the Paleo-Tethys was opened (Fig. 11b). At the same time, Laurentia, Baltica and Avalonia were assembled, forming Laurussia. During the Devonian, the Sarıcakaya Massif was at middle to lower crustal depths, and was intruded by biotite-hornblende tonalite and two mica granites probably due to a southward subduction beneath Armorica, which was initiated probably during Early Devonian (Fig. 11c). During Carboniferous time, the Rheic Ocean was consumed, and the Sakarya Zone (Armorica) collided with Laurussia (Fig. 11d). This process is associated with the development of Early to Late Carboniferous high-temperature/low pressure metamorphism and voluminous Carboniferous granite and gabbro intrusions.

10. Conclusions

The biotite-metagranite and amphibolite within the Sarıcakaya Massif (Sakarya Zone, NW Turkey) have Silurian igneous crystallization ages. They have intruded into a clastic sequence of Cambro-Ordovician age. This Silurian acidic and basic magmatism in concert with the sporadic presence of Ordovican-Silurian detrital zircons from various metaclastic rocks of Late Paleozoic and Early Mesozoic ages suggest that Silurian magmatism is common in subsurface throughout the Sakarya Zone. Geochemically, the amphibolite displays anorogenic tholeiitic to alkaline affinity, and was derived from melts from depleted mantle sources, while biotite-metagranite from crustal melts. They probably formed during the detachment of the Sakarya Zone from the northern margin of Gondwana, thus indicating an initial opening of the Paleo-Tethys. During the Early Carboniferous, the clastic sequence and the intruding granite and gabbro were subjected to high-temperature/middle to low-pressure amphibolite-facies metamorphism.

Supplementary data to this article can be found online at https://doi.org/10.1016/j.lithos.2019.105302.

Declaration of competing interest

The authors declare that they have no conflict of interest.

Acknowledgements

We have greatly benefited from discussions with A. M. Celâl Şengör and for constructive reviews by Iain Neill and Abdurrahman Dokuz. Financial supports from research foundation of the istanbul Teknik Üniversitesi (#8629 and #9853) are gratefully acknowledged. Both Gültekin Topuz and Aral I. Okay acknowledge financial support from Turkish Academy of Science (TÜBA). Helps of Andrew R. C. Kylander-Clark, Ezgi Sağlam, Turgut Duzman, Ümitcan Erbil, Mutlu Özkan and İrfan Yolcubal during sample preparation and measurements are gratefully acknowledged. Fırat Şengün is thanked for help during data reduction. We thank Nalan Lom for sharing her compilation on the Paleozoic magmatism in the European Variscides. Special thanks go to Yaşar Sürü and Yaşar Sürü for their logistic help during the field work.

References

Akal, C., Candan, O., Koralay, O.E., Oberhänsli, R., Chen, F., Prelević, D., 2012. Early Triassic potassic volcanism in the Afyon Zone of the Anatolides/Turkey: implications for the rifting of the Neo-Tethys. Int. J. Earth Sci. 101, 177–194.

Antić, M., Peytcheva, I., von Quadt, A., Kounov, A., Trivić, B., Serafimovski, T., Tasev, G., Gerdjikov, I., Wetzel, A., 2016. Pre-Alpine evolution of a segment of the North-Gondwanan margin: geochronological and geochemical evidence from the central Serbo-Macedonian Massif. Gondwana Res. 36, 523–544.

Aysal, N., Ustaömer, T., Öngen, A.S., Keskin, M., Köksal, S., Peytcheva, I., Fanning, M., 2012a. Origin of the Early-Middle Devonian magmatism in the Sakarya Zone, NW Turkey: geochronology, geochemistry and isotope systematics. J. Asian Earth Sci. 45, 201–222.

Aysal, N., Öngen, A.S., Peytcheva, I., Keskin, M., 2012b. Origin and evolution of the Havran unit, western Sakarya basement (NW Turkey): new LA-ICP-MS U-Pb dating of the metasedimentary-metagranitic rocks and possible affiliation to Avalonian microcontinent. Geodin. Acta 25, 226–247.

Casas, J.M., Castiñeiras, P., Navidad, M., Liesa, M., Carreras, J., 2010. New insights into the Late Ordovician magmatism in the Eastern Pyrenees: U–Pb SHRIMP zircon data from the Canigó massif. Gondwana Res. 17, 317–324.

Cliff, R.A., 1980. U–Pb isotopic evidence from zircons for lower Palaeozoic tectonic activity in the Austroalpine nappe the Eastern Alps. Contrib. Mineral. Petrol. 71, 283–288.

Dokuz, A., 2011. A slab detachment and delamination model for the generation of Carboniferous high-potassium I-type magmatism in the Eastern Pontides, NE Turkey: the Köse composite pluton. Gondwana Res. 19, 926–944.

Dokuz, A., Külekçi, E., Aydınçakır, E., Kandemir, R., Alçiçek, M.C., Pecha, M.E., Sünnetçi, K., 2017. Cordierite-bearing strongly peraluminous Cebre rhyolite from the eastern Sakarya Zone, NE Turkey: constraints on the Variscan orogeny. Lithos 278, 285–302.

Dombrowski, A., Henjest-Kunst, F., Höhndorf, A., Kröner, A., Okrusch, M., Richter, P., 1995. Orthogneiss in the Spessart crystalline complex, northwest Bavaria, Silurian magmatism at an active continental margin. Geol. Rundsch. 83, 399–411.

Dunkl, I., Mikes, T., Simon, K., von Eynatten, H., 2008. Brief introduction to the Windows program Pepita: data visualization, and reduction, outlier rejection, calculation of trace element ratios and concentrations from LA-ICP-MS data. In: Sylvester, P. (Ed.), Laser Ablation ICP-MS in the Earth Sciences: Current Practices and Outstanding Issues. Mineralogical Association of Canada, pp. 334–340.

Franke, W., 2000. The mid-European segment of the Variscides: tectonostratigraphic units, terrane boundaries and plate tectonic evolution. Geol. Soc. Lond. Spec. Publ. 179, 35–61.

Göncüoğlu, M.C., Turhan, N., Şentürk, K., Özcan, A., Uysal, Ş., Yalınız, M.K., 2000. A geotraverse across Northwestern Turkey: tectonic units of the Central Sakarya region and their tectonic evolution. Geol. Soc. Lond. Spec. Publ. 173, 139–161.

Göncüoğlu, M.C., Turhan, N., Tekin, U.K., 2003. Evidence for the Triassic rifting and opening of the Neotethyan Izmir-Ankara Ocean and discussion on the presence of Cimmerian events at the northern edge of the Tauride-Anatolide Platform, Turkey. Boll. Soc. Geol. Ital. 203–212 Special vol. 2.

Himmerkus, F., Reischmann, T., Kostopoulos, D., 2009. Serbo-Macedonian revisited: a Silurian basement terrane from northern Gondwana in the Internal Hellenides, Greece. Tectonophysics 473, 20–35.

Horstwood, M.A., Kosler, J., Gehrels, G., Jackson, S.E., McLean, N.M., Paton, C., Pearson, N.J., Sircombe, K., Sylvester, P., Vermeesch, P., Bowring, J.F., Condon, D.J., Schoene, B., 2016. Community-derived standards for LA-ICP-MS U-(Th-)Pb geochronology- uncertainty propagation, age interpretation and data reporting. Geostand. Geoanal. Res. 40, 311–332.

İlbeyli, N., Demirbilek, M., Kibici, Y., 2015. Geochemistry and petrogenesis of the Late Paleozoic magmatism in the Sakarya Zone (NW Turkey). Neues Jb. Mineral. Abh. 192, 177–194.

Karslı, O., Dokuz, A., Kandemir, R., 2017. Subduction-related Late Carboniferous to Early Permian Magmatism in the Eastern Pontides, the Camlik and Casurluk plutons: Insights from geochemistry, whole-rock Sr–Nd and in situ zircon Lu–Hf isotopes, and U–Pb geochronology. Lithos 266–267, 98–114.

Kaygusuz, A., Arslan, M., Sipahi, F., Temizel, İ., 2016. U–Pb zircon chronology and petrogenesis of Carboniferous plutons in the northern part of the Eastern Pontides, NE Turkey: constraints for Paleozoic magmatism and geodynamic evolution. Gondwana Res. 39, 327–346.

Kozur, H., 1998. The age of the siliciclastic series (Karareis Formation) of the western Karaburun Peninsula, western Turkey. Paleontologia Polonica 58, 171–189.

Kroner, U., Romer, R.L., 2013. Two plates—many subduction zones: the Variscan orogeny reconsidered. Gondwana Res. 24, 298–329.

Kylander-Clark, A.R.C., Hacker, B.R., Cottle, J.M., 2013. Laser-ablation split-stream ICP petrochronology. Chem. Geol. 345, 99–112.

Matte, P., 2001. The Variscan collage and orogeny (480–290 Ma) and the tectonic definition of the Armorica microplate: a review. Terra Nova 13, 122–128.

Mayringer, F., Treloar, P.J., Gerdes, A., Finger, F., Shengelia, D., 2011. New age data from the Dzirula massif, Georgia: implications for the evolution of the Caucasian Variscides. Am. J. Sci. 311, 404–441.

Nance, R.D., Linnemann, U., 2008. The Rheic Ocean: origin, evolution, and significance. GSA Today 18, 4–12.

Neubauer, F., 2002. Evolution of late Neoproterozoic to early Paleozoic tectonic elements in Central and Southeast European Alpine mountain belts: review and synthesis. Tectonophysics 352, 87–103.

Nowell, G.M., Kempton, P.D., Noble, S.R., Fitton, J.G., Saunders, A.D., Mahoney, J.J., Taylor, R.N., 1998. High precision Hf isotope measurements of MORB and OIB by thermal ionization mass spectrometry: insights into the depleted mantle. Chem. Geol. 149, 211–233.
Nzegge, O.M., Satır, M., Siebel, W., Taubald, H., 2006. Geochemical and isotopic constraints on the genesis of the Late Palaeozoic Deliktaş and Sivrikaya granites from the Kastamonu granitoid belt (Central Pontides, Turkey). Neues Jb. Mineral. Abh. 183, 27–40.
Okay, A.I., 2000. Was the Late Triassic orogeny in Turkey caused by the collision of an oceanic plateau? In: Bozkurt, E., Winchester, J.A., Piper, J.D.A. (Eds.), Tectonic and Magmatism in Turkey and Surrounding Area. Geological Society of London. Vol. 173, pp. 25–41 Special Publication
Okay, A.I., Leven, E.Ja., 1996. Stratigraphy and paleontology of the Upper Paleozoic sequences in the Pulur (Bayburt) region, Eastern Pontides. Turk. J. Earth Sci. 5, 145–155.
Okay, A.I., Nikishin, A., 2015. Tectonic evolution of the southern margin of Laurasia in the Black Sea region. Int. Geol. Rev. 57, 1051–1076.
Okay, A.I., Şahintürk, Ö., 1997. Geology of the eastern pontides. In: Robinson, A.G. (Ed.), Regional and Petroleum Geology of the Black Sea and Surrounding Region, pp. 291–311 American Association of Petroleum Geologists (AAPG) Memoir No. 68.
Okay, A.I., Topuz, G., 2017. Variscan orogeny in the Black Sea region. Int. J. Earth Sci. 106, 569–592.
Okay, A.I., Satır, M., Maluski, H., Siyako, M., Monie, P., Metzger, R., Akyüz, S., 1996. In: Yin, A., Harrison, M. (Eds.), Paleo- and Neo-Tethyan events in northwest Turkey: geological and geochronological constraints. Tectonics of Asia, Cambridge University Press, pp. 420–441.
Okay, A.I., Satır, M., Shang, C.K., 2008a. Ordovician metagranitoid from the Anatolide-Tauride block, northwest Turkey: geodynamic implications. Terra Nova 20, 280–288.
Okay, A.I., Bozkurt, E., Satır, M., Yiğitbaş, E., Crowley, Q.G., Shang, C.K., 2008b. Defining the southern margin of Avalonia in the Pontides: geochronological data from the Late Proterozoic and Ordovician granitoids from NW Turkey. Tectonophysics 461, 252–264.
Okay, A.I., Satir, M., Zattin, M., Cavazza, W., Topuz, G., 2008c. An Oligocene ductile strike-slip shear zone: the Uludağ Massif, northwest Turkey—implications for the westward translation of Anatolia. Geol. Soc. Am. Bull. 120, 893–911.
Okay, A.I., Noble, P.J., Tekin, U.K., 2011. Devonian radiolarian ribbon cherts from the Karakaya Complex, Northwest Turkey: implications for the Paleo-Tethyan evolution. C. R. Palevol 10, 1–10.
Othman, M., 2017. Petrogenesis of the Sarıcakaya Intrusive Rocks (Eskişehir, NW Turkey) and Their Implications. İstanbul Teknik Üniversitesi, Avrasya Yer Bilimleri Enstitüsü, p. 55 Unpublished master thesis.
Özbey, Z., Ustaömer, T., Robertson, A.H.F., Ustaömer, P.A., 2013. Tectonic significance of Late Ordovician granitic magmatism and clastic sedimentation on the northern margin of Gondwana (Tavşanlı Zone, NW Turkey). J. Geol. Soc. Lond. 170, 159–173.
Palme, H., O'Neill, H.S.C., 2014. Cosmochemical estimates of mantle composition. Treatise Geochem. 3, 1–38.
Passchier, C.W., Trouw, R.A.J., 2005. Deformation mechanisms. Microtectonics, 2nd Springer, Berlin.
Paton, C., Hellstrom, J., Paul, B., Woodhead, J., Hergt, J., 2011. Iolite: freeware for thevisualization and processing of mass spectrometric data. J. Anal. At. Spectrom. 26, 2508–2518.
Pearce, J.A., 1996. A user's guide to basalt discrimination diagrams. In: Wyman, D.A. (Ed.), Trace Element Geochemistry of Volcanic Rocks: Applications for Massive Sulphide Exploration, pp. 79–113 Geological Association of Canada, Short Course Notes 12.
Pearce, J.A., 2008. Geochemical fingerprinting of oceanic basalts with applications to ophiolite classification and the search for Archean oceanic crust. Lithos 100, 14–48.
Pearce, J.A., 2014. Immobile element fingerprinting of ophiolites. Elements 10, 101–108.
Pearce, J.A., Norry, M.J., 1979. Petrogenetic implications of Ti, Zr, Y, and Nb variations in volcanic rocks. Contributions to Mineralogy and Petrology 69, 33–47.
Polat, A., Hofmann, A.W., Münker, C., Regelous, M., Appel, P.W., 2003. Contrasting geochemical patterns in the 3.7–3.8 Ga pillow basalt cores and rims, Isua greenstone belt, Southwest Greenland: implications for postmagmatic alteration processes. Geochimica et Cosmochimica Acta 67, 441–457.
Putiš, M., Ivan, P., Milan Kohút, M., Spišiak, J., Siman, P., Radvanec, M., Uher, P., Sergeev, S., Larionov, A., Méres, Š., Demko, R., Ondrejka, M., 2009. Metaigneous rocks of the West-Carpathian basement, Slovakia: indicators of early Paleozoic extension and shortening events. Bull. Soc. Géol. Fr. 180, 461–471.
Reischmann, T., Anthes, G., 1996. Geochronologie und geodynamische Entwicklung der Mitteldeutschen Kristallinschwelle westlich des Rheins. Terra Nostra 96, 161–162.
Rolland, Y., 2017. Caucasus collisional history: review of data from East Anatolia to West Iran. Gondwana Res. 49, 130–146.
Rolland, Y., Sosson, M., Adamia, S., Sadradze, N., 2011. Prolonged Variscan to Alpine history of an active Eurasian margin (Georgia, Armenia) revealed by $^{40}Ar/^{39}Ar$ dating. Gondwana Res. 20, 798–815.
Rubatto, D., Schaltegger, U., Lombardo, D., Colombo, F., Compagnoni, R., 2001. Complex Paleozoic magmatic and metamorphic evolution in the Argentera massif (Western Alps), resolved with U-Pb dating. Schweiz. Mineral. Petrogr. Mitt. 81, 213–228.
Schmid, S.M., Fügenschuh, B., Kounov, A., Matenco, L., Nievergelt, P., Oberhansli, R., Pleuger, J., Schefer, S., Schuster, R., Tomljenovich, B., Ustaszewski, K., 2019. Tectonic units of the Alpine collision zone between eastern Alps and western Turkey. Gondwana Res. (in press).
Schoene, B., Crowley, J.L., Condon, D.J., Schmitz, M.D., Bowring, S.A., 2006. Reassessing the uranium decay constants for geochronology using ID-TIMS U-Pb data. Geochim. Cosmochim. Acta 70, 426–445.
Schulz, B., Bombach, K., Pawlig, S., Brätz, H., 2004. Neoproterozoic to Early-Palaeozoic magmatic evolution in the Gondwana-derived Austroalpine basement to the south of the Tauern Window (Eastern Alps). Int. J. Earth Sci. 93, 824–843.
Segal, I., Halicz, L., Platzner, I.T., 2003. Accurate isotope ratio measurements of ytterbium by multiple collection inductively coupled plasma mass spectrometry applying erbium and hafnium in an improved double external normalization procedure. J. Anal. At. Spectrom. 18, 1217–1223.
Şengör, A.M.C., Yılmaz, Y., 1981. Tethyan evolulution of Turkey: a plate tectonic approach. Tectonophysics 75, 181–241.
Shervais, J.W., 1982. Ti-V plots and the petrogenesis of modern and ophiolitic lavas. Earth Planet. Sci. Lett. 59, 101–118.
Somin, M.L., 2011. Pre-jurassic basement of the greater caucasus: brief overview. Turk. J. Earth Sci. 20, 545–611.
Sommermann, A.E., Anderle, H.-J., Todt, W., 1994. Das Alter des Quarzkeratophyrs der Krausaue bei Rüdesheim am Rhein (Blatt 6013 Bingen, Rheinisches Schiefergebirge). Geol. Jahrb. Hess. 122, 143–157.
Stampfli, G.M., Borel, G.D., 2002. A plate tectonic model for the Paleozoic and Mesozoic constrained by dynamic plate boundaries and restored synthetic oceanic isochrones. Earth Planet. Sci. Lett. 196, 17–33.
Stampfli, G.M., Hochard, C., Vérard, C., Wilhelm, C., von Raumer, J., 2013. The formation of Pangea. Tectonophysics 593, 1–19.
Sunal, G., 2013. Devonian magmatism in the western Sakarya Zone, Karacabey region, NW Turkey. Geodin. Acta 25, 183–201.
Sunal, G., Satır, M., Natal'in, B.A., Toraman, E., 2008. Paleotectonic position of the Strandja Massif and surrounding continental blocks based on zircon Pb-Pb age studies. Int. Geol. Rev. 50, 519–545.
Topuz, G., Altherr, R., 2004. Pervasive rehydration of granulites during exhumation – an example from the Pulur complex, Eastern Pontides, Turkey. Mineral. Petrol. 81, 165–185.
Topuz, G., Altherr, R., Kalt, A., Satır, M., Werner, O., Schwarz, W.H., 2004a. Aluminous granulites from the Pulur complex, NE Turkey: a case of partial melting, efficient melt extraction and crystallization. Lithos 72, 183–207.
Topuz, G., Altherr, R., Satır, M., Schwarz, M., 2004b. Low grade metamorphic rocks from the Pulur complex, NE Turkey: implications for pre-Liassic evolution of the Eastern Pontides. Int. J. Earth Sci. 93, 72–91.
Topuz, G., Altherr, R., Schwarz, W.H., Dokuz, A., Meyer, H.-P., 2007. Variscan amphibolite-facies metamorphic rocks from the Kurtoğlu metamorphic complex (Gümüşhane area, Eastern Pontides, Turkey). Int. J. Earth Sci. 96, 861–873.
Topuz, G., Altherr, R., Siebel, W., Schwarz, W.H., Zack, T., Hasözbek, A., Barth, M., Satır, M., Şen, C., 2010. Carboniferous high-potassium I-type granitoid magmatism in the Eastern Pontides: the Gümüşhane pluton (NE Turkey). Lithos 116, 92–110.
Topuz, G., Göçmengil, G., Rolland, Y., Çelik, Ö., Zack, T., Schmitt, A.K., 2013a. Jurassic accretionary complex and ophiolite from northeast Turkey: no evidence for the Cimmerian continental ribbon. Geology 45, 255–258.
Topuz, G., Candan, O., Zack, T., Yılmaz, A., 2017. East Anatolian plateau constructed over a continental basement: No evidence for the East Anatolian accretionary complex. Geology 45 (9), 791–794. https://doi.org/10.1130/G39111.1.
Topuz, G., Çelik, Ö., Şengör, A.M.C., Altıntaş, İ., Zack, T., Rolland, Y., Barth, M., 2013b. Jurassic ophiolite formation and emplacement as backstop to a subduction-accretion complex in northeast Turkey, the Refahiye ophiolite, and relation to the Balkan ophiolites. Am. J. Sci. 313, 1054–1087.
Topuz, G., Okay, A.I., Altherr, R., Schwarz, W.H., Siebel, W., Zack, T., Satır, M., Şen, C., 2011. Post-collisional adakite-like magmatism in the Ağvanis Massif and implications for the evolution of the Eocene magmatism in the Eastern Pontides (NE Turkey). Lithos 125, 131–150.
Topuz, G., Okay, A.I., Altherr, R., Schwarz, W.H., Sunal, G., Altınkaynak, L., 2014. Triassic warm subduction in northeast Turkey: evidence from the Ağvanis metamorphic rocks. Island Arc 23, 181–205.
Topuz, G., Okay, A.I., Schwarz, W.-H., Sunal, G., Altherr, A., Kylander-Clark, A.R.C., 2018. A middle Permian ophiolite fragment in Late Triassic greenschist- to blueschist-facies rocks in NW Turkey: an additional pulse of suprasubduction-zone ophiolite formation in the Tethyan belt? Lithos 300–301, 121–135.
Uğurcan, O.G., Ustaömer, T., Gerdes, A., 2019. Cambrian-Early Ordovician Magmatism, Mid-Late Paleozoic Sedimentation and Early Carboniferous Metamorphism in the Central Sakarya Terrane; Sakarya Zone, NW Turkey. International Earth Science Colloquium on the Aegean Region 2019 EASCA Izmir. p. 11.
Ustaömer, T., Robertson, A.H.F., Ustaömer, P.A., Gerdes, A., Peytcheva, I., 2012a. Constraints on Variscan and Cimmerian magmatism and metamorphism in the Pontides (Yusufeli–Artvin area), NE Turkey from U–Pb dating and granite geochemistry. Geol. Soc. Lond. Spec. Publ. 372, 49–74.
Ustaömer, P.A., Ustaömer, T., Robertson, A.H.F., 2012b. Ion probe U-Pb dating of the Central Sakarya basement: a peri-Gondwana terrane intruded by Late Lower Carboniferous subduction/collision-related granitic rocks. Turk. J. Earth Sci. 21, 905–932.
Ustaömer, T., Ustaömer, P.A., Robertson, A.H.F., Gerdes, A., 2016. Implications of U-Pb and Lu-Hf isotopic analysis of detrital zircons for the depositional age, provenance and tectonic setting of the Permian-Triassic Palaeotethyan Karakaya Complex, NW Turkey. Int. J. Earth Sci. 105, 7–38.
Uzunçimen, S., Tekin, U.K., Bedi, Y., Perincek, D., Varol, E., Soycan, H., 2011. Discovery of the Late Triassic (Middle Carnian–Rhaetian) radiolarians in the volcano-sedimentary sequences of the Kocali Complex, SE Turkey: correlation with the other Tauride units. J. Asian Earth Sci. 40, 180–200.
Vermeesch, P., 2018. IsoplotR: a free and open toolbox for geochronology. Geosci. Front. 9, 1479–1493.
von Raumer, J.F., Stampfli, G.M., 2008. The birth of the Rheic Ocean—Early Palaeozoic subsidence patterns and subsequent tectonic plate scenarios. Tectonophysics 461, 9–20.
von Raumer, J.F., Bussy, F., Schaltegger, U., Schulz, B., Stampfli, G.M., 2013. Pre-Mesozoic Alpine basements—their place in the European Paleozoic framework. GSA Bull. 125, 89–108.
Winchester, J.A., the PACE TMR Network Team (contract ERBFMRXCT97-0136), 2002. Palaeozoic amalgamation of Central Europe: new results from recent geological and geophysical investigations. Tectonophysics 360, 5–21.